Recognition of Z-RNA by ADAR1 limits interferon responses

Qiannan Tang[1], Rachel E. Rigby[1,†], George R. Young[2,†], Astrid Korning-Hvidt[1], Tiong Kit Tan[1], Anne Bridgeman[1], Alain R. Townsend[1,3], George Kassiotis[4,5] & Jan Rehwinkel[1,*]

[1]Medical Research Council Human Immunology Unit, Medical Research Council Weatherall Institute of Molecular Medicine, Radcliffe Department of Medicine, University of Oxford, Oxford, OX3 9DS, UK.
[2]Retrovirus–Host Interactions, The Francis Crick Institute, London, UK.
[3]Centre for Translational Immunology, Chinese Academy of Medical Sciences Oxford Institute, University of Oxford, Oxford, UK.
[4]Retroviral Immunology, The Francis Crick Institute, London, UK.
[5]Department of Infectious Disease, Faculty of Medicine, Imperial College London, London, UK.

*correspondence: jan.rehwinkel@imm.ox.ac.uk

[†]These authors contributed equally.

Keywords

ADAR1, Zα domain, Z-RNA, MDA5, MAVS, interferon, influenza A virus

Running Title

Z-RNA recognition by ADAR1

Abstract

Nucleic acids are powerful triggers of innate immunity and can adopt the unusual Z-conformation. The p150 isoform of adenosine deaminase acting on RNA 1 (ADAR1) prevents aberrant interferon (IFN) induction and contains a Z-nucleic acid binding (Zα) domain. We report that knock-in mice bearing two point mutations in the Zα domain of ADAR1, which abolish binding to Z-form nucleic acids, spontaneously induced type I IFNs and IFN-stimulated genes (ISGs) in multiple organs. This included the lung where both stromal and haematopoietic cells displayed ISG induction in *Adar1*$^{mZ\alpha/mZ\alpha}$ mice. Concomitantly, *Adar1*$^{mZ\alpha/mZ\alpha}$ mice showed improved control of influenza A virus. The spontaneous IFN response in *Adar1*$^{mZ\alpha/mZ\alpha}$ mice required MAVS, implicating cytosolic RNA sensing. Finally, analysis of A-to-I changes revealed a specific requirement of ADAR1's Zα domain in editing of a subset of RNAs. In summary, our results reveal that endogenous RNAs in Z-conformation have immunostimulatory potential that is curtailed by ADAR1.

Introduction

The innate immune system monitors the intra- and extracellular environments for unusual nucleic acids (Bartok and Hartmann, 2020). This process, known as 'nucleic acid sensing', detects pathogen invasion and disturbances to homeostasis. It involves a large number of germline encoded nucleic acid sensors. Upon engagement by immunostimulatory DNA or RNA, these sensors signal to initiate a large spectrum of responses, including transcription of the genes encoding type I interferons (IFNs). Type I IFNs – secreted cytokines that act in paracrine and autocrine manner – induce expression of hundreds of IFN-stimulated genes (ISGs). The proteins encoded by ISGs mediate a plethora of functions and include antiviral effectors (Schoggins, 2019). Sustained type I IFN responses can have detrimental effects and cause a range of diseases including the neuroinflammatory Aicardi-Goutières Syndrome (AGS) (Uggenti et al., 2019). It is therefore important to understand the molecular mechanisms that prevent activation of nucleic acid sensors by 'normal' DNA and RNA present in healthy cells (Bartok and Hartmann, 2020).

We and others proposed that double-stranded (ds) nucleic acids adopting an unusual conformation known as Z-DNA/RNA activate innate immunity (Maelfait et al., 2017; Sridharan et al., 2017; Zhang et al., 2020b). Z-DNA was initially described by Alexander Rich (Wang et al., 1979). Unlike canonical B-DNA, a right-handed double helix, Z-DNA is a left-handed double helix with a zig-zag-shaped phosphodiester back bone (Wang et al., 1979). dsRNA can also adopt the Z-conformation (Davis et al., 1986; Hall et al., 1984). Biological functions of Z nucleic acids, in particular those of Z-RNA, are incompletely understood (Herbert, 2019). A small number of proteins, all involved in innate immunity, contain Z-DNA/RNA binding domains known as Zα domains (Athanasiadis, 2012). These domains specifically bind to and stabilise Z-

DNA/RNA, or induce the Z-conformation (Athanasiadis, 2012; Brown et al., 2000; Kim et al., 2018; Schwartz et al., 1999).

There are two mammalian proteins with Zα domains: Z-DNA binding protein 1 (ZBP1) and adenosine deaminase acting on RNA 1 (ADAR1, also known as DRADA1). ZBP1 contains two Zα domains that have been suggested to recognise viral and endogenous Z-RNAs (Devos et al., 2020; Jiao et al., 2020; Maelfait et al., 2017; Sridharan et al., 2017; Wang et al., 2020; Zhang et al., 2020b). Binding to Z-RNA activates ZBP1 and results in the induction of necroptosis, an inflammatory form of cell death (Maelfait et al., 2020).

ADAR1 has two splice isoforms: ADAR1-p110, which is constitutively expressed and localised in the cell nucleus, and ADAR1-p150 that is IFN-inducible and present in the nucleus and cytosol. Both isoforms contain a C-terminal deaminase domain that converts adenosine to inosine in dsRNA, a process known as A-to-I RNA editing. Conversion of adenosine to inosine in protein-coding sequences can lead to incorporation of non-synonymous amino acids during translation due to base pairing of inosine with cytosine. However, the vast majority of A-to-I editing events occur in non-coding RNAs (Eisenberg and Levanon, 2018; Reich and Bass, 2019). This includes transcripts from repetitive elements (REs), particularly *Alu* elements and short interspersed nuclear elements (SINEs) in human and mouse, respectively. Both ADAR1 isoforms further contain three dsRNA binding domains (dsRBDs) and a so-called Zβ domain. Zβ adopts a fold similar to Zα domains but does not bind Z-form nucleic acids due to substitutions of key amino acids (Athanasiadis et al., 2005; Kim et al., 2003). ADAR1-p150 has an extended N-terminus harbouring a Zα domain (Heraud-Farlow and Walkley, 2020).

ADAR1 deficiency results in profound inflammatory phenotypes. In human, germline *ADAR1* mutations cause AGS (Rice et al., 2012). These mutations predominantly map to the deaminase domain; however, one mutation encoding

p.Pro193Ala is found in the Zα domain. Pro193 contributes to Z-form nucleic acid binding (Schwartz et al., 1999) and changing it to Ala reduces RNA editing in a reporter assay (Mannion et al., 2014). *Adar1*$^{-/-}$ mice, editing-deficient *Adar1*$^{E861A/E861A}$ knock-in animals and *Adar1*$^{p150-/p150-}$ mice, which only lack ADAR1-p150, all die *in utero* (Hartner et al., 2004; Liddicoat et al., 2015; Wang et al., 2004; Ward et al., 2011). Akin to spontaneous type I IFN induction in AGS patients with *ADAR1* mutation, *Adar1*$^{-/-}$ and *Adar1*$^{E861A/E861A}$ embryos display profound type I IFN responses prior to death (Hartner et al., 2009; Liddicoat et al., 2015). Multiple nucleic acid sensors mediate the anti-proliferative, cell death and type I IFN phenotypes observed in ADAR1-deficient settings: the oligoadenylate synthetase (OAS)–RNase L system (Li et al., 2017), protein kinase R (PKR) (Chung et al., 2018; Li et al., 2010) and melanoma differentiation-associated protein 5 (MDA5) (Liddicoat et al., 2015; Mannion et al., 2014; Pestal et al., 2015). Upon activation by dsRNA, OAS proteins synthesise 2'-5' oligoadenylate, a second messenger that in turn activates RNase L, resulting in widespread RNA degradation. PKR also detects dsRNA and represses protein translation. Both effects have been proposed to explain lethality of ADAR1-deficient cells (Chung et al., 2018; Li et al., 2017). Induction of type I IFNs in ADAR1-deficient mice and human cells is mediated by the RNA sensor MDA5, that signals via its adaptor mitochondrial antiviral-signalling protein (MAVS) (Bajad et al., 2020; Chung et al., 2018; Guallar et al., 2020; Liddicoat et al., 2015; Mannion et al., 2014; Pestal et al., 2015).

These observations suggest a model in which endogenous dsRNAs are stabilised in ADAR1-deficient cells due to the absence of RNA editing and are then recognised by RNA sensors (Dias Junior et al., 2019; Eisenberg and Levanon, 2018) . Indeed, some ADAR1 substrates such as transcripts from *Alu* elements base-pair to form duplex structures, which are predicted to be destabilised by inosine : uracil mismatches introduced by RNA editing (Ahmad

et al., 2018; Chung et al., 2018; Pfaller et al., 2018; Song et al., 2020). This concept has been tested experimentally in an RNase protection assay: transcripts spanning *Alu* elements in inverted orientation are protected by recombinant MDA5 protein in RNA samples extracted from ADAR1-deficient cells (Ahmad et al., 2018; Mehdipour et al., 2020).

How the different nucleic acid binding domains in ADAR1 select and recruit RNA substrates for subsequent editing is unknown. In light of (i) emerging roles of Z-form nucleic acids in innate immunity (Kesavardhana and Kanneganti, 2020), (ii) the MAVS-dependent phenotype of *Adar1*$^{p150-/p150-}$ mice (Pestal et al., 2015), and (iii) natural occurrence of the p.Pro193Ala mutation in AGS patients (Rice et al., 2012), we interrogated Z-form nucleic acid binding by the Zα domain in ADAR1-p150. Here, we report the generation of knock-in mice bearing two missense mutations in the Zα domain, which prevent nucleic acid binding. Although these *Adar1*$^{mZ\alpha/mZ\alpha}$ mice were developmentally normal and fertile, they displayed spontaneous induction of type I IFNs and ISGs in multiple organs and cell types. This phenotype was dependent on MAVS and conferred partial protection against influenza A virus (IAV) infection. Analysis of sequencing data revealed that ~8% of RNA editing events in wild-type (WT) cells required a functional ADAR1-p150 Zα domain. Taken together, our study delineates the function of the Zα domain in ADAR1-p150 *in vivo* and suggests that recognition of Z-form RNA by ADAR1 contributes to the suppression of IFN responses.

Results

Generation of Zα domain mutated mice

To study the role of Z-form nucleic acid binding to the Zα domain in ADAR1-p150 in an *in vivo* setting, we generated knock-in mice bearing two missense mutations: p.Asn175Ala and p.Tyr179Ala. These residues are conserved and are homologous to Asn173 and Tyr177 in human ADAR1; they were chosen because of their essential role in Z-form nucleic acid binding (Feng et al., 2011; Li et al., 2009; Schade et al., 1999; Schwartz et al., 1999). Given the embryonic lethality of *Adar1*$^{p150-/p150-}$ mice (Ward et al., 2011), we opted for a conditional knock-in strategy (Figure S1A). The Zα domain is encoded by exon 2 of the *Adar1* gene. In brief, we introduced in inverted orientation into the intron between exons 2 and 3 a mutated copy of exon 2 (designated 2*) containing four nucleotide substitutions, changing both Asn175 and Tyr179 to Ala. We flanked exons 2 and 2* with LoxP and Lox2272 sites such that Cre-mediated recombination removes exon 2 and flips exon 2* into forward orientation (Figure S1A). We designated the conditional allele '*fl-mZα*' and the recombined allele expressing mutant Adar1 '*mZα*'. To determine the impact of the Zα domain mutations when present in all cells and tissues, we crossed *Adar1*$^{+/fl-mZα}$ mice with a line expressing Cre recombinase under control of the ubiquitously active *Pgk* promoter. The resulting *Adar1*$^{+/mZα}$ mice were intercrossed to generate homozygous animals. We validated the presence of the mutations by sequencing and found that *Adar1*$^{mZα/mZα}$ animals were born at expected mendelian ratios (Figure S1B and S1C). Furthermore, they developed normally and were fertile. The mutations introduced into the Zα domain did not alter the expression of the two isoforms of ADAR1 in bone marrow-derived myeloid cells (BMMCs) (Figure S1D). Taken together, Z-form nucleic acid binding by ADAR1-p150 is not essential for survival at whole organism level.

175

176 Mutation of the Zα domain in ADAR1-p150 triggers a multi-organ type I IFN
177 response

178 We tested whether *Adar1*$^{mZ\alpha/mZ\alpha}$ mice display spontaneous activation of
179 type I IFNs as was reported in ADAR1-deficient settings. We collected lung,
180 liver and spleen tissues and extracted RNA for RT-qPCR analysis. Transcript
181 levels of *Ifnb1* (encoding IFNβ) were elevated in lung RNA samples from
182 *Adar1*$^{mZ\alpha/mZ\alpha}$ mice (Figure 1A). Moreover, the ISG transcripts *Ifit1* and *Ifi44* were
183 expressed at higher levels in all three organs from Zα domain mutated animals
184 (Figure 1A). This gene expression signature was type I IFN-specific: tissues
185 from *Adar1*$^{mZ\alpha/mZ\alpha}$ mice contained comparable mRNA levels of *Ifng*, *Tnfa* and
186 *Il1b* (encoding IFNγ, TNFα and pro-IL-1β), with only a minor increase of *Tnfa*
187 mRNA in lung (Figure 1A). We validated the ISG signature at protein level by
188 analysing expression of interferon stimulated gene 15 (ISG15) in whole lung
189 lysates. ISG15 is a ubiquitin-like modifier that is induced by IFN and is
190 conjugated to target proteins in a process called ISGylation (Perng and
191 Lenschow, 2018). Western blot showed that lung lysates from *Adar1*$^{mZ\alpha/mZ\alpha}$
192 mice contained increased amounts of monomeric ISG15 as well as increased
193 levels of ISGylated proteins, visible as a high-molecular weight smear (Figure
194 1B).

195 We next analysed different types of cultured primary cells from WT and
196 *Adar1*$^{mZ\alpha/mZ\alpha}$ mice. We observed heightened ISG expression in Zα domain
197 mutated lung fibroblasts (Figure 1C). In contrast, comparable levels of ISG
198 transcripts were found in WT and *Adar1*$^{mZ\alpha/mZ\alpha}$ BMMCs, as well as in mouse
199 embryonic fibroblasts (MEFs) (Figure 1D, E). This indicates that ISG induction
200 may be cell-type specific.

201 Among the organs we analysed, lung exhibited the most profound ISG
202 signature, and spontaneous ISG induction was also observed in cultured lung

fibroblasts (Figure 1A, D). We therefore focused on the lung for the next set of experiments. We used RNA extracted from lung for RNA sequencing to obtain a global view of gene expression in *Adar1*$^{mZ\alpha/mZ\alpha}$ mice. We found that 99 protein coding genes were differentially expressed by at least 2-fold in mutant lungs, including 89 upregulated and 10 downregulated transcripts (Figure 2A). 40% of the induced mRNAs were encoded by ISGs; this included well-known factors such as *Irf7*, *Cxcl10*, *Zbp1* and *Usp18* (Figure 2A). We used gene ontology (GO) analysis of biological processes to further classify upregulated genes. GO terms related to type I IFNs and anti-viral defence were enriched amongst genes induced in *Adar1*$^{mZ\alpha/mZ\alpha}$ lungs (Figure 2B). The most highly enriched GO category, regulation of ribonuclease activity, included many *Oas* transcripts, which are known to be IFN-inducible (Schoggins, 2019).

We also analysed REs in our RNA sequencing data and found 540 induced and 112 repressed REs (Figure 2C and Table S1). SINEs were underrepresented amongst differentially expressed REs, whilst long terminal repeat (LTR) elements were enriched (Figure 2C). Dysregulation of REs has been reported in settings of inflammation and can be driven by IFNs (Chuong et al., 2016). Taken together, these data show that the lungs of Zα domain mutated animals displayed a type I IFN-driven gene signature.

Stromal and haematopoietic cells contribute to the ISG signature in the lungs of *Adar1*$^{mZ\alpha/mZ\alpha}$ mice

To identify the type of cell(s) that display the ISG signature in the lungs of *Adar1*$^{mZ\alpha/mZ\alpha}$ mice, we used magnetic-activated cell sorting (MACS) to isolate haematopoietic cells, marked by CD45 expression, and stromal cells lacking this marker. There was no difference in the proportions of haematopoietic and stromal cells between WT and *Adar1*$^{mZ\alpha/mZ\alpha}$ lungs (Figure 3A). We confirmed the purity of MACS-enriched haematopoietic and stromal cells to be >97%

(Figure S2). We then extracted RNA for RT-qPCR analysis of ISGs and found that both lung haematopoietic and stromal cells displayed ISG induction (Figure 3B). For the three ISGs tested, fold inductions in *Adar1*$^{mZ\alpha/mZ\alpha}$ samples were similar in CD45+ and CD45- cells (Figure 3B). However, it is noteworthy that baseline ISG levels appeared to be lower in haematopoietic cells compared to stromal cells (Figure 3B).

Next, we analysed ISG expression in different types of lung haematopoietic and stromal cells. Using two staining panels and fluorescence-activated cell sorting (FACS), we obtained eight different populations of CD45+ cells, including B cells, T cells, dendritic cells (DCs), monocytes, macrophages, NK cells, neutrophils and eosinophils (Figure S3). There were no differences between WT and *Adar1*$^{mZ\alpha/mZ\alpha}$ mice in the proportions of these cell populations, with the exception of DCs, which were less abundant in the mutant lungs (Figure S3A). *Ifit1*, *Ifit2* and *Isg15* were significantly induced in neutrophils from the lungs of *Adar1*$^{mZ\alpha/mZ\alpha}$ mice (Figure 4A, B). However, these ISGs showed no, or limited and statistically insignificant, upregulation in other types of CD45+ cells (Figure 4A, B). In contrast, the ISGs *Ifi44* and *Oas1a* were upregulated in multiple haematopoietic cell types (Figure 4A, B). Transcripts encoding type I IFNs were undetectable by RT-qPCR in all samples analysed (data not shown). Several ISGs, including *Ifit1*, *Ifit2* and *Isg15*, are not only induced by IFNAR signalling but can also be upregulated by IRF3/7, independent of type I IFN-initiated JAK-STAT activation (Ashley et al., 2019; DeFilippis et al., 2006; Goubau et al., 2009; Grandvaux et al., 2002; Lazear et al., 2013). Induction of this ISG-subset can therefore occur in a cell-autonomous manner, for example when aberrant nucleic acids are sensed by pattern recognition receptors (PRRs) that signal via IRF3/7. Other ISGs, including *Ifi44* and *Oas1a*, are only induced via IFNAR signalling (Lazear et al., 2013). Therefore, our observation that *Ifit1*, *Ifit2* and *Isg15* were primarily induced in neutrophils, while *Ifi44* and *Oas1a* were

upregulated more broadly (Figure 4A, B), suggests that *Adar1*$^{mZ\alpha/mZ\alpha}$ neutrophils may autonomously activate IRF3. We further speculate that the ISG signature in other haematopoietic cells such as B cells may be due to paracrine type I IFN signalling via IFNAR.

We also analysed the lung stromal compartment and isolated by FACS endothelial and epithelial cells using CD31 and CD326 as markers, respectively (Figure S4). We further isolated CD45- cells lacking these markers; this mixed population likely included fibroblasts and other cell types. We observed induction of *Ifit1*, *Isg15* and *Ifi44* in *Adar1*$^{mZ\alpha/mZ\alpha}$ cells of all three populations analysed (Figure 4C). It is therefore likely that, in addition to neutrophils, multiple non-haematopoietic cells initiate type I IFN production in the lungs of *Adar1*$^{mZ\alpha/mZ\alpha}$ mice.

Haematopoietic cells are sufficient to induce ISGs in *Adar1*$^{mZ\alpha/mZ\alpha}$ mice

To further dissect the cellular requirements for ISG induction in *Adar1*$^{mZ\alpha/mZ\alpha}$ mice, we generated bone marrow (BM) chimeric animals. Lethally irradiated *Cd45.1* WT recipients were reconstituted with *Cd45.2* BM from WT or *Adar1*$^{mZ\alpha/mZ\alpha}$ animals (Figure S5A). We found reconstitution levels of the haematopoietic compartment to be about 90% by analysing cell surface levels of CD45.1 and CD45.2 on white blood cells from recipient mice (Figure S5B). Similar levels of reconstitution were observed in the lung (Figure S5C). We first obtained RNA from whole lung tissue for RT-qPCR analysis. The ISGs *Ifit1*, *Oas1a* and *Zbp1* were upregulated in *Adar1*$^{mZ\alpha/mZ\alpha}$→WT chimeras compared to WT→WT chimeras (Figure 4D, “Total”). This indicates that *Adar1*$^{mZ\alpha/mZ\alpha}$ BM-derived cells triggered an IFN response in WT animals. We also isolated different cell populations from the lungs of chimeric animals by FACS (see Figure S3 for gating), extracted RNA and performed RT-qPCR. *Ifit1* and *Ifit2* mRNA levels were significantly induced in neutrophils from *Adar1*$^{mZ\alpha/mZ\alpha}$→WT

287 chimeras, but not in B cells and CD45- cells (Figure 4D). In contrast, *Oas1a*
288 and/or *Zbp1* were upregulated in multiple cell populations including CD45- cells,
289 neutrophils and B cells (Figure 4D). These observations are consistent with the
290 results shown in Figure 4A and 4B and indicate that neutrophils may initiate
291 type I IFN production that then results in ISGs induction in other cell types.
292 Taken together, *Adar1*$^{mZ\alpha/mZ\alpha}$ haematopoietic cells were sufficient to induce
293 ISGs in the lungs of WT mice.
294
295 IAV replication is inhibited in *Adar1*$^{mZ\alpha/mZ\alpha}$ mice
296 In light of the spontaneous type I IFN response in *Adar1*$^{mZ\alpha/mZ\alpha}$ mice, we
297 next asked whether these Zα domain mutant mice were protected against viral
298 infection. ISGs upregulated in the lungs of *Adar1*$^{mZ\alpha/mZ\alpha}$ mice included factors
299 such as *Ifit1* and *Zbp1* that are known to control IAV (Pichlmair et al., 2011;
300 Zhang et al., 2020b) (Figure 2A). We intranasally infected WT and *Adar1*$^{mZ\alpha/mZ\alpha}$
301 mice with the H3N2 strain of recombinant IAV (A-X31; A/HongKong/1/1968)
302 using a dose that caused moderate weight loss. WT animals lost about 10%
303 body weight from day 3 until day 7 after infection, and subsequently recovered
304 their weight (Figure 5A). In contrast, *Adar1*$^{mZ\alpha/mZ\alpha}$ mice gained weight until day
305 4 after infection (Figure 5A). This was followed by weight loss on days 5-7,
306 which slightly exceeded weight loss in WT mice, and recovery from day 8
307 onwards. These observations suggest that *Adar1*$^{mZ\alpha/mZ\alpha}$ mice were protected
308 against IAV at an early stage of the infection.
309 We further characterised early IAV infection in *Adar1*$^{mZ\alpha/mZ\alpha}$ mice at day 3
310 after inoculation. We calculated a 'lung index' (lung weight/body weight x100;
311 Luo et al., 2012) and found this marker of pathology and inflammation to be
312 significantly higher in infected WT mice compared to *Adar1*$^{mZ\alpha/mZ\alpha}$ animals
313 (Figure 5B). Next, we analysed viral loads by determining the levels of the viral
314 *NP* and *M* transcripts by RT-qPCR. Compared to infected WT lungs, levels of

315 these viral RNAs were reduced in infected *Adar1*$^{mZ\alpha/mZ\alpha}$ lungs (Figure 5C).
316 Concomitantly, mRNA levels of *Ifnb1*, *Ifng*, *Il1b*, *Tnfa* and *Il6*, as well as IL6
317 protein, were strongly induced in infected WT lungs, and these effects were
318 curtailed in *Adar1*$^{mZ\alpha/mZ\alpha}$ lungs (Figure 5D, E). In sum, IAV replication and virus-
319 induced inflammation were reduced in *Adar1*$^{mZ\alpha/mZ\alpha}$ animals.
320
321 ISG induction in *Adar1*$^{mZ\alpha/mZ\alpha}$ mice is MAVS-dependent
322 We next investigated which nucleic acid sensing pathway triggered
323 spontaneous ISG expression in *Adar1*$^{mZ\alpha/mZ\alpha}$ mice. Since ADAR1-deficiency
324 results in activation of the MDA5-MAVS pathway (Liddicoat et al., 2015;
325 Mannion et al., 2014; Pestal et al., 2015), we hypothesised that the ISG
326 signature in *Adar1*$^{mZ\alpha/mZ\alpha}$ mice was driven by MAVS. To test this, we crossed
327 *Adar1* mutant mice with MAVS knock-out animals to generate *Adar1*$^{mZ\alpha/mZ\alpha}$;
328 *Mavs*$^{-/-}$ mice. Loss of MAVS prevented the ISG induction observed in
329 *Adar1*$^{mZ\alpha/mZ\alpha}$ lungs, livers and spleens (Figure 6A). Because of the
330 neuropathology observed in patients with AGS, we also analysed brain tissue.
331 *Adar1*$^{mZ\alpha/mZ\alpha}$ mice showed elevated *Ifnb1* expression and a pronounced ISG
332 signature in the brain (Figure 6B). Akin to the situation in other tissues, these
333 effects were fully MAVS-dependent (Figure 6B). Taken together, the Zα domain
334 of ADAR1-p150 was involved in preventing MAVS-mediated IFN induction,
335 implicating a role in limiting activation of MDA5 or RIG-I.
336
337 The Zα domain of ADAR1-p150 is required for editing of a subset of RNAs
338 Human ADAR1-p150 bearing the p.Pro193Ala mutation shows reduced
339 editing activity in a reporter assay (Mannion et al., 2014). To identify natural
340 RNA substrates edited by ADAR1-p150 in a Zα domain-dependent manner, we
341 analysed our RNA sequencing data from WT and *Adar1*$^{mZ\alpha/mZ\alpha}$ lungs for A→G
342 transitions. These are indicative of A-to-I RNA editing as inosine pairs with

343 cytosine during reverse transcription. The most sensitive and specific method
344 for annotating this mutational profile compares the fit of Dirichlet models of
345 observed base frequencies between test and control samples (Piechotta et al.,
346 2017). We extended this methodology to allow comparisons of biological
347 replicates, to incorporate the orientation of the originating RNA (revealed by our
348 stranded RNAseq protocol), to include fine-grained filtering of potential editing
349 sites, and to add a 'detection' step, whereby observed base frequencies at
350 potential editing sites are additionally compared to a model of the per-base error
351 rate obtained *de novo* from the dataset.

352 Considered individually, for each of the three WT and three *Adar1*$^{mZ\alpha/mZ\alpha}$
353 lung samples analysed, we detected ~35,000-40,000 editing sites (Figure 7A).
354 Considered as biological replicates, increasing statistical robustness, 40,342
355 and 46,164 sites were identified that were shared amongst all three WT or
356 *Adar1*$^{mZ\alpha/mZ\alpha}$ lung samples, respectively. These 'detected' sites had a median
357 editing level of ~10% in both WT and *Adar1*$^{mZ\alpha/mZ\alpha}$ samples (Figure 7B). This
358 shows that there was no global defect in RNA editing in *Adar1*$^{mZ\alpha/mZ\alpha}$ mice.

359 We further defined 'differential' sites as those that were 'detected' in the WT
360 samples and showed higher (>2-fold) levels of editing than in *Adar1*$^{mZ\alpha/mZ\alpha}$ mice.
361 3,249 sites (8% of sites 'detected' in WT) were 'differential' and displayed ~9%
362 median editing in WT lungs, which was strongly reduced for the majority of sites
363 in *Adar1*$^{mZ\alpha/mZ\alpha}$ mice (Figure 7B). Read depth was equivalent between
364 'detected' and 'differential' sites (data not shown), excluding the possibility that
365 lack of editing in *Adar1*$^{mZ\alpha/mZ\alpha}$ samples was simply due to reduced sequence
366 coverage. We then attempted to understand whether these Zα domain-
367 dependent sites were characterised by unique properties. First, we annotated
368 editing sites to 5' untranslated regions (UTRs), coding sequences (CDSs),
369 3'UTRs, intronic and intergenic regions (Figure 7C). The majority of editing sites
370 'detected' in WT samples were found in intronic regions (~83%). 3'UTRs

accounted for ~11% of edits and intergenic regions contained ~5% of sites. Less than 1% of sites mapped to 5'UTRs and CDSs. The annotation of 'differential' sites was similar with a small increase in intronic sites (~86%), while 8% of 'differential' edits were found in 3'UTRs.

Given that many A-to-I RNA editing events are known to occur in repetitive elements (REs) (Eisenberg and Levanon, 2018), we analysed the enrichment of editing events in WT samples, by computing observed versus expected numbers, for each RE class (Figure 7D). This analysis showed that editing events were greatly enriched within SINEs (Figure 7D) and further showed that, with the exception of the B4 family, all SINE sub-families exhibited enrichment, albeit to varying degrees (Figure S6A). Furthermore, there were no large-scale differences between the SINEs represented when comparing 'detected' and 'differential' sites (Figure S6B), suggesting that all SINEs had equal potential to contribute sites that were differentially edited between WT and *Adar1*$^{mZ\alpha/mZ\alpha}$ mice.

We next analysed the genomic distance of edited SINEs to another SINE in inverted orientation. In human, transcripts spanning inverted repeat *Alu* elements have been suggested to form duplex RNA structures recognised by ADAR1 and MDA5 (Ahmad et al., 2018; Mehdipour et al., 2020). Compared to all SINEs, we found that edited SINEs were closer to another SINE in inverted orientation (Figure 7E), although there was no difference between SINEs containing 'detected' (in WT samples) and 'differential' sites. Taken together, these data demonstrate that a subset consisting of about 8% of editing sites required a functional ADAR1-p150 Zα domain for efficient A-to-I conversion.

Discussion

Although Z-nucleic acids were discovered ~40 years ago, little is known to this date about their biological activities. This is in part due to their thermodynamic properties: the B- and A-conformations of dsDNA and dsRNA, respectively, are energetically favoured compared to the Z-conformation, making Z-DNA and Z-RNA difficult to study (Herbert, 2019). The formation of Z-DNA has been proposed to release torsional strain induced by the movement of polymerases (Wittig et al., 1992; Wolfl et al., 1995). Physiological functions of Z-RNA have remained enigmatic until recently. We and others proposed that Z-RNA is recognised by ZBP1 in settings of viral infection and autoinflammation, resulting in the induction of programmed cell death (Devos et al., 2020; Jiao et al., 2020; Maelfait et al., 2017; Sridharan et al., 2017; Wang et al., 2020; Zhang et al., 2020b).

Here, we studied ADAR1-p150 that like ZBP1 contains a Zα domain specialised in binding to Z nucleic acids. We report spontaneous induction of type I IFNs *in vivo* upon introduction of mutations into the ADAR1-p150 Zα domain that prevent binding to Z-DNA/RNA. This effect was observed in multiple organs and cell types from *Adar1*$^{mZ\alpha/mZ\alpha}$ mice and required MAVS. These data show that RIG-I-like receptors were activated by endogenously generated Z-RNAs, and that editing of these Z-RNAs by ADAR1-p150 limited the response. We therefore reveal type I IFN induction as a new biological function of Z-RNA.

Our computational analysis mapped ~40,000 editing sites in lung RNA samples from WT mice. These sites were enriched in SINEs but not in other classes of REs. Furthermore, we found that edited SINEs were more likely to be in proximity to another SINE in inverted orientation. These results agree with previous findings demonstrating that editing sites are enriched in non-coding sequences containing self-complementary regions predicted to form duplex

RNA structures (Eisenberg and Levanon, 2018; Porath et al., 2017; Solomon et al., 2017; Tan et al., 2017).

Importantly, we revealed that ~8% of editing sites detected in WT samples required a functional ADAR1-p150 Zα domain. This subset of Zα-dependent sites mapped to genomic features and REs similarly to all detected sites. To characterise whether the sequences surrounding Zα-dependent editing sites have a propensity to form Z-RNA, we analysed sequences 500 nt up- and down-stream of editing sites. We tested GC content, given that GC-repeats have a higher tendency to adopt the Z-conformation (Davis et al., 1986). There was no enrichment of GC dinucleotides, or other motifs, around differentially edited sites compared to all detected sites (data not shown). We also used the Z-hunt algorithm (Champ et al., 2004; Ho et al., 1986) to predict the likelihood of sequences around editing sites to form the Z-conformation. In parallel, we calculated the distance of editing sites to genomic regions predicted by SIBZ to form the Z-conformation (Zhabinskaya and Benham, 2011). Neither computational approach revealed differences between 'detected' and 'differential' sites. It is noteworthy that both algorithms were developed for dsDNA and may be unsuitable for predicting the Z-conformation in RNA. Future studies will be required to dissect the properties the Zα-dependent RNA editing sites.

We also found diminished editing in WT samples at ~14% of the sites detected as edited in *Adar1*$^{mZ\alpha/mZ\alpha}$ mice (data not shown). ADAR1-p150 is encoded by an ISG and *Adar1* transcript levels increased by 1.6-fold in *Adar1*$^{mZ\alpha/mZ\alpha}$ lungs (data not shown). Thus, it is likely that type I IFN-induced expression of ADAR1-p150 in mutant mice and recruitment of A-form dsRNAs via the dsRBDs explains editing at these sites.

ADAR1 mutations in human cause AGS and include the missense p.Pro193Ala mutation in the Zα domain. Interestingly, this *ADAR1* allele is

common with frequencies of up to ~1/160 (www.ensembl.org) (Mannion et al., 2014). In AGS patients, homozygous p.Pro193Ala mutation has not been observed; instead, this mutation occurs together with other *ADAR1* mutations (Rice et al., 2012). It is therefore likely that *ADAR1* p.Pro193Ala is hypomorphic and does not cause disease when present homozygously. Consistent with this notion, we found that *Adar1*$^{mZ\alpha/mZ\alpha}$ mice did not have any gross abnormalities and were fertile. These mice nonetheless displayed type I IFN and ISG induction in multiple organs. This included the lung and bestowed protection against IAV infection at early stages. It is therefore conceivable that the *ADAR1* p.Pro193Ala variant has been maintained in humans by providing a selective advantage during viral infections due to elevated expression of antiviral factors at baseline.

It is noteworthy in this context that anti- and pro-viral functions of ADAR1 have been reported. ADAR1 limits or controls replication of several viruses, including measles virus, members of *Paramyxoviridae* family, IAV, HIV-1, vesicular stomatitis virus and Hepatitis delta virus (Casey, 2012; Li et al., 2010; Vogel et al., 2020; Ward et al., 2011; Weiden et al., 2014). However, for other viruses such as Zika and KSHV, ADAR1 has been shown to facilitate replication (Zhang et al., 2020a; Zhou et al., 2019). It will be interesting for future studies to determine the role of the *ADAR1* variants unable to bind Z nucleic acids in these viral infections.

ADAR1 has recently emerged as a promising target for cancer treatment. If expressed by transformed cells *in vitro* or by tumours *in vivo*, ADAR1 protects against both cell death and anti-cancer immune responses (Gannon et al., 2018; Ishizuka et al., 2019; Liu et al., 2019). Loss of ADAR1 in cancer cells results in death or reduced growth and sensitises to immunotherapy. Interestingly, the protective effects appear to depend on ADAR1-p150 (Gannon et al., 2018; Ishizuka et al., 2019). It is therefore possible that endogenous Z-RNAs induce

anti-cancer effects upon ADAR1 loss. Future studies should test this, for example by reconstitution of ADAR1-p150 mutants unable to bind Z-RNA. Furthermore, development of inhibitors that target the Zα domain of ADAR1, the Zα - Z-RNA interaction or Z-RNA formation should be considered. Compared to deaminase inhibitors, such 'Z-inhibitors' would have the advantage of specifically targeting the p150 isoform, avoiding possible detrimental consequences of targeting ADAR1-p110 (Pestal et al., 2015).

In addition to the activation of MDA5, loss of ADAR1 also results in activation of the OAS-RNaseL system and PKR. The latter may be particularly important in cancer settings (Gannon et al., 2018; Ishizuka et al., 2019; Liu et al., 2019). Although PKR activation results in a global shutdown of translation, some proteins are selectively made and mediate the integrated stress response (Pakos-Zebrucka et al., 2016). These include the transcription factor ATF4 that induces stress-response genes. We observed moderate induction of some ATF4-dependent genes (Harding et al., 2003) including *Asns* (1.3-fold), *Slc7a5* (1.3-fold), *Slc7a11* (1.9-fold) and *Mthfd2* (1.7-fold) (data not shown). It is therefore possible that editing of Z-RNA by ADAR1-p150 limits not only type I IFN induction but also PKR-dependent stress responses.

In conclusion, we discovered MAVS-dependent type I IFN induction as a biological function of Z-RNA that is curtailed by ADAR1-p150. These insights are not only of fundamental value but also have important implications for understanding and modulating detrimental and beneficial type I IFN responses in autoinflammation and cancer.

Materials and Methods

Mice

Adar1$^{+/fl\text{-}mZ\alpha}$ mice were generated by Cyagen. In brief, genomic fragments containing homology arms were amplified from a BAC and were sequentially assembled into a targeting vector together with recombination sites and selection markers as shown in Figure S1A. Successful assembly of the targeting vector was verified by restriction digest and sequencing. The linearised vector was subsequently delivered to ES cells (C57BL/6) via electroporation, followed by drug selection, PCR screening and sequencing. After confirming correctly targeted ES clones via Southern blotting, we selected clones for blastocyst microinjection, followed by chimera production. Founders were confirmed as germline-transmitted via crossbreeding with WT animals. The Neo cassette was flanked by Rox sites and contained a Dre recombinase controlled by a promoter active in the germline, resulting in deletion of the Neo cassette in F1 animals (Figure S1A). These *Adar1*$^{+/fl\text{-}mZ\alpha}$ mice were further crossed with *Pgk-Cre* mice provided by Samira Lakhal-Littleton to produce *Adar1*$^{+/mZ\alpha}$ animals (Figure S1A). The following PCR primers were used for genotyping:

F, 5'-TGACGAGAGACTTGTTTTCCTAGCATG-3',

R1, 5'-TGCCTCAATGAGACCTCCAACTTAACTC-3',

R2^{WT}, 5'-CAGGGAGTACAAAATACGATT-3', and

R2^{MUT}, 5'-CAGGGAGGCCAAAATACGAGC-3'.

PCR with primers F and R1 yielded a product of 357 bp for the WT *Adar1* allele and a 421 bp product for both '*fl-mZ*α' and '*mZ*α' alleles. PCR with primers F and R2^{WT} resulted in 1095 and 1158 bp products for the WT and 'fl-*mZ*α' alleles, respectively, and no product for the '*mZ*α' allele. Finally, PCR with primers F and R2^{MUT} resulted in a 1158 bp product for the '*mZ*α' allele only.

Mavs$^{-/-}$ mice were a gift from C. Reis e Sousa and were originally from J. Tschopp (Michallet et al., 2008). All mice were on the C57BL/6 background. This work was performed in accordance with the UK Animal (Scientific Procedures) Act 1986 and institutional guidelines for animal care. This work was approved by project licenses granted by the UK Home Office (PPL numbers PC041D0AB, PBA43A2E4 and P79A4C5BA) and was also approved by the Institutional Animal Ethics Committee Review Board at the University of Oxford.

Cell culture

Lung fibroblasts and MEFs were grown in DMEM and BMMCs in RPMI, as described previously (Li et al., 2013; Maelfait et al., 2017). Media were supplemented with 10% heat-inactivated FCS and 2 mM L-glutamine; for BMMCs, 200 U/ml recombinant mouse GM-CSF (Peprotech) was added. MEFs were cultured at 3% oxygen.

RNA extraction and RT-qPCR

Organs collected from freshly killed mice (8-10 weeks of age) were snap frozen in liquid nitrogen immediately after dissection and stored at -80°C until further processing. Organs were homogenised with glass beads (425-600 μm, Sigma-Aldrich) in TRIzol (Thermo Fisher Scientific) using a FastPrep F120 instrument (Thermo Savant). RNA was extracted following the manufacturer's instructions and further purified using RNeasy Plus columns (Qiagen) including a gDNA eliminator column step. cDNA synthesis was performed with SuperScript II reverse transcriptase (Thermo Fisher Scientific) with random hexamer (Qiagen) or oligo $(dT)_{12\text{-}18}$ (Thermo Fisher Scientific) as primers. qPCR was done using Taqman Universal PCR Mix (Thermo Fisher Scientific) and Taqman probes (Applied Biosystems). Alternatively, qPCR was performed

559 using EXPRSS SYBR GreenER qPCR Supermix (Thermo Fisher Scientific)
560 and DNA oligonucleotides (Sigma Aldrich). qPCR was performed on a
561 QuantStudio 7 Flex real-time PCR system (Applied Biosystem). The qPCR
562 probes and primers used in this study are listed in Table S2.
563
564 *In vivo* infection
565 WT and *Adar1*$^{mZ\alpha/mZ\alpha}$ mice were used at 8-10 weeks of age. Mice were
566 intranasally inoculated with 50 μl X31 (0.04 haemagglutination units (HAU))
567 diluted in viral growth medium (VGM; DMEM with 1% bovine serum albumin
568 (Sigma-Aldrich A0336), 10 mM HEPES buffer, penicillin (100 U/ml) and
569 streptomycin (100 μg/ml)) or mock infected with 50 μl VGM under light
570 isoflurane anaesthesia. Animals were assessed daily for weight loss and signs
571 of disease. Mice reaching 20% weight loss were euthanised.
572
573 Western Blot
574 Cells were lysed in RIPA buffer (50 mM Tris.HCl, pH7.4; 150 mM NaCl; 1%
575 NP-40 (Sigma-Aldrich), 0.5% Deoxycholate, 0.1% SDS and Complete protease
576 inhibitor (Roche)) at 4°C for 10 minutes. Protein lysates were then cleared by
577 centrifugation at 13000 rpm for 10 minutes. Samples were mixed with NuPAGE
578 SDS-PAGE sample loading buffer (ThermoFisher) containing 10% 2-
579 mercaptoethanol. A primary antibody against ADAR1 was purchased from
580 Santa Cruz (sc-73408). The antibody recognising ISG15 was a gift from Klaus-
581 Peter Knobeloch. HRP-coupled secondary antibodies were from GE
582 Healthcare.
583
584 Flow cytometry
585 Lungs from 8-10 week old mice were dissected and mechanically disrupted
586 using scissors before incubation in RPMI containing 1 μg/ml type II collagenase

(Worthington Biochemical Corporation) and 40 U/ml DNase I (Sigma Aldrich) at 37°C for 60 minutes, with resuspension after 30 minutes to facilitate tissue dissociation. Cells were filtered through a 70 μm cell strainer (BD Falcon), rinsed with RPMI and pelleted at 400 x g for 5 minutes. The cell pellet was resuspended in 5 ml RBC lysis buffer (Qiagen), incubated at room temperature for 5 minutes and then washed twice with 45 ml RPMI. Cells were resuspended in 500 μl FACS buffer (PBS containing 10% (v/v) FCS and 2 mM EDTA) and passed through a 70 μm cell strainer. Viable cells were counted using a haemocytometer. Cells were washed with PBS before incubation with LIVE/DEAD Fixable Aqua Dead Cell Stain (Invitrogen) diluted 1:200 in PBS for 30 minutes at room temperature. Cells were washed once with FACS buffer and then stained with surface antibodies diluted 1:200 in Brilliant buffer (BD Biosciences) for 30 minutes. Cells were sorted directly into TRIzol-LS Reagent (Thermo Fisher Scientific) on BD FACSAria II and III machines (BD Biosciences). Alternatively, $1.5x10^6$ cells were stained and analysed using an Attune NxT Flow Cytometer (Thermo Fisher Scientific). Data were analysed using FlowJo (v10.6.2).

Magnetic cell fraction

Cells from lungs were prepared as described above. 10^7 cells were resuspended in 90 μl of MACS buffer (PBS containing 0.5% BSA and 2 mM EDTA) and then incubated with 10 μl of CD45 microbeads (Miltenyi) for 15 minutes. The mixture was then washed with MACS buffer and resuspend in 500 μl MACS buffer for magnetic separation on MACS LS columns (Miltenyi) according to the manufacturer's instructions. Cells were recovered from the flow-through (CD45-) and column (CD45+). 10% of cells were stained and analysed by FACS to confirm purity. The remaining cells were pelleted, resuspend in TRIzol (ThermoFisher) and processed for RT-qPCR.

615

616 Bone marrow chimera

617 B6.SJL-CD45.1 mice were used as bone marrow recipients and were
618 lethally irradiated twice (4.5 Gy for 300 seconds, separated by a ~3 hour rest).
619 Mice were then injected intravenously with bone marrow from either WT
620 (CD45.2) or *Adar1*$^{mZ\alpha/mZ\alpha}$ mice. Recipient mice received antibiotics (0.16
621 mg/mL, Enrofloxacin (Baytril), Bayer Corporation) in drinking water for four
622 weeks following irradiation and were rested for >8 weeks before tissue
623 collection.

624

625 RNA-seq and data processing

626 Stranded Illumina sequencing libraries were prepared with the RNA-Seq
627 Ribozero kit from isolated RNAs and submitted for PE150 sequencing using an
628 Illumina NovaSeq6000 machine, yielding ~100M reads per sample.
629 Sequencing data was processed using a Nextflow v20.07 (Di Tommaso et al.,
630 2017) pipeline automating quality control using FastQC v0.11.8
631 (bioinformatics.babraham.ac.uk/projects/fastqc/), quality and adapter trimming
632 using cutadapt v1.18 (Martin, 2011), contaminant detection using screen.sh
633 (within BBMap v36.20, sourceforge.net/projects/bbmap/), strand-aware
634 alignment using HISAT2 v2.1.0 (Kim et al., 2019) and STAR v2.7.1a (Dobin
635 et al., 2013), post-alignment quality-assurance using 'gene body coverage',
636 'transcript integrity', and 'inner distance' metrics from RSeQC v2.6.4 (Wang et
637 al., 2012), and strand-specific counting of uniquely-mapping reads using
638 featureCounts (within Subread v1.6.4, (Liao et al., 2014)) against Ensembl
639 GRCm38.100 annotations. Additional, unstranded counts were obtained with
640 featureCounts against a database of repetitive elements previously prepared
641 for GRCm38 (Attig et al., 2017) using reads unassigned to features during the
642 previous step.

643

644 Differential expression analysis

645 Downstream differential expression analysis was conducted using counts
646 obtained for STAR read mappings using DESeq2 (Love et al., 2014) (v1.22.1)
647 within R (v4.0.2). Gene ontology analysis was performed using goseq (Young
648 et al., 2010) (1.34.1). Heatmaps were generated using the pheatmap package
649 (v1.0.12).

650

651 Detection of A-to-I editing

652 A Python 3.8 program, edIted (github.com/A-N-Other/pedestal), was
653 produced to identify editing sites. edIted performs stranded assessments of
654 RNA editing from samtools mpileup (Li, 2011) data, building on the Dirichlet-
655 based models implemented in ACCUSA2 and JACUSA (Piechotta and
656 Dieterich, 2013; Piechotta et al., 2017). When run with test data alone, edIted
657 runs in 'detect' mode, finding base modifications by comparing the goodness of
658 fit of Dirchlet models of the base error (derived from the Phred quality data in
659 the mpileup input) and the background sequencing error to the base
660 frequencies recorded at a specific position. With an additional control dataset,
661 edIted runs in 'differential' mode, performing the above analysis to determine
662 significantly edited sites before additionally testing for differential editing by
663 comparing the goodness of fit of Dirichlet models of the base error from the test
664 and control datasets to their own and each other's base frequencies. When
665 biological replicates are provided, edIted adjusts the reported Z scores to reflect
666 the proportion of test dataset samples displaying editing. edIted was run in both
667 modes with samtools mpileup files (supplemented with TS tag metadata)
668 separately for HISAT2 and STAR alignments of the data with the flags '--
669 min_depth 5 --min_alt_depth 2 --min_edited 0.01 --max_edited 0.9 --z_score
670 2.58'. For differential analyses the '--min_fold 2' flag was used and, where

considering biological replicates the '--reps 3' flag, such that editing is required in all three samples. All analyses were conducted supplying BED files of ENCODE blacklisted regions (Amemiya et al., 2019) and known splice sites (regions set to splice site +/- 2 nts) to the '--blacklist' flag. Sites that were found in common between the HISAT2- and STAR-mapped data were retained for further analysis.

Analysis of A-to-I editing sites

Sites obtained from edIted were assigned to genomic features using annotatr v1.16 within R (Cavalcante and Sartor, 2017). Assessments of editing enrichment within repetitive elements were conducted using regioneR v1.22 within R (Gel et al., 2016) using randomization-based permutation tests with 100 bootstraps. Assessment of distance to neighbouring inverted SINE super-family (B1, B2, B3, B4) members was conducted with bedtools v2.29.2 closest (Quinlan and Hall, 2010) using the '-io -S' flags. Outputs and the detailed statistics were produced with GraphPad Prism v8.

ELISA

Mouse IL-6 was quantified by uncoated ELISA Kit (ThermoFisher) according to manufacturer's instruction.

691 **Author contributions** (using the CRediT taxonomy)

692 Conceptualisation: Q.T. and J.R.; Methodology: Q.T., R.E.R. and G.Y.; Software:
693 R.E.R. and G.Y.; Validation: Q.T. and J.R.; Formal analysis: Q.T., R.E.R., G.Y.
694 and J.R.; Investigation: Q.T., R.E.R., G.Y., A.K.H., T.K.T. and A.B.; Resources:
695 A.T. and G.K.; Data curation: Q.T., R.E.R. and G.Y.; Writing – Original Draft:
696 Q.T., G.Y. and J.R.; Writing – Review & Editing: all authors; Visualisation: Q.T.,
697 R.E.R., G.Y. and J.R.; Supervision: J.R., A.T., and G.K.; Project administration:
698 Q.T.; Funding acquisition: J.R.

699

700 **Acknowledgments**

701 The authors thank P. Shing Ho and Craig Benham for providing access to the
702 Z-hunt and SIBZ codes, respectively. We further thank Daniel Stetson, Andrew
703 Oberst, Jonathan Maelfait, Caetano Reis e Sousa, David Ron, Annemarthe van
704 Der Veen and members of the Rehwinkel lab for discussion. The authors thank
705 Ziqi Long and Oliver Bannard for their help with generating BM chimeras.
706 This work was funded by the UK Medical Research Council [MRC core funding
707 of the MRC Human Immunology Unit; J.R.], the Wellcome Trust [grant number
708 100954; J.R.], the Lister Institute [J.R.] and the Francis Crick Institute [G.K.],
709 which receives its core funding from Cancer Research UK, the UK Medical
710 Research Council, and the Wellcome Trust. T.K.T. was funded by the
711 Townsend-Jeantet Charitable Trust (charity number 1011770) and the EPA
712 Cephalosporin Early Career Researcher Fund. The funders had no role in study
713 design, data collection and analysis, decision to publish, or preparation of the
714 manuscript.

715

716 **Declaration of interests**

717 The authors have declared that no conflict of interest exits.

References

Ahmad, S., Mu, X., Yang, F., Greenwald, E., Park, J.W., Jacob, E., Zhang, C.Z., and Hur, S. (2018). Breaching Self-Tolerance to Alu Duplex RNA Underlies MDA5-Mediated Inflammation. Cell *172*, 797-810 e713.

Amemiya, H.M., Kundaje, A., and Boyle, A.P. (2019). The ENCODE Blacklist: Identification of Problematic Regions of the Genome. Sci Rep *9*, 9354.

Ashley, C.L., Abendroth, A., McSharry, B.P., and Slobedman, B. (2019). Interferon-Independent Upregulation of Interferon-Stimulated Genes during Human Cytomegalovirus Infection is Dependent on IRF3 Expression. Viruses *11*.

Athanasiadis, A. (2012). Zalpha-domains: at the intersection between RNA editing and innate immunity. Seminars in cell & developmental biology *23*, 275-280.

Athanasiadis, A., Placido, D., Maas, S., Brown, B.A., 2nd, Lowenhaupt, K., and Rich, A. (2005). The crystal structure of the Zbeta domain of the RNA-editing enzyme ADAR1 reveals distinct conserved surfaces among Z-domains. Journal of molecular biology *351*, 496-507.

Attig, J., Young, G.R., Stoye, J.P., and Kassiotis, G. (2017). Physiological and Pathological Transcriptional Activation of Endogenous Retroelements Assessed by RNA-Sequencing of B Lymphocytes. Frontiers in microbiology *8*, 2489.

Bajad, P., Ebner, F., Amman, F., Szabo, B., Kapoor, U., Manjali, G., Hildebrandt, A., Janisiw, M.P., and Jantsch, M.F. (2020). An internal deletion of ADAR rescued by MAVS deficiency leads to a minute phenotype. Nucleic acids research *48*, 3286-3303.

Bartok, E., and Hartmann, G. (2020). Immune Sensing Mechanisms that Discriminate Self from Altered Self and Foreign Nucleic Acids. Immunity *53*, 54-77.

Brown, B.A., 2nd, Lowenhaupt, K., Wilbert, C.M., Hanlon, E.B., and Rich, A. (2000). The zalpha domain of the editing enzyme dsRNA adenosine deaminase binds left-handed Z-RNA as well as Z-DNA. Proceedings of the National Academy of Sciences of the United States of America *97*, 13532-13536.

Casey, J.L. (2012). Control of ADAR1 editing of hepatitis delta virus RNAs. Curr Top Microbiol Immunol *353*, 123-143.

Cavalcante, R.G., and Sartor, M.A. (2017). annotatr: genomic regions in context.

753 Bioinformatics *33*, 2381-2383.

754 Champ, P.C., Maurice, S., Vargason, J.M., Camp, T., and Ho, P.S. (2004).
755 Distributions of Z-DNA and nuclear factor I in human chromosome 22: a model
756 for coupled transcriptional regulation. Nucleic acids research *32*, 6501-6510.

757 Chung, H., Calis, J.J.A., Wu, X., Sun, T., Yu, Y., Sarbanes, S.L., Dao Thi, V.L.,
758 Shilvock, A.R., Hoffmann, H.H., Rosenberg, B.R., and Rice, C.M. (2018).
759 Human ADAR1 Prevents Endogenous RNA from Triggering Translational
760 Shutdown. Cell *172*, 811-824 e814.

761 Chuong, E.B., Elde, N.C., and Feschotte, C. (2016). Regulatory evolution of
762 innate immunity through co-option of endogenous retroviruses. Science *351*,
763 1083-1087.

764 Davis, P.W., Hall, K., Cruz, P., Tinoco, I., Jr., and Neilson, T. (1986). The
765 tetraribonucleotide rCpGpCpG forms a left-handed Z-RNA double-helix.
766 Nucleic Acids Res *14*, 1279-1291.

767 DeFilippis, V.R., Robinson, B., Keck, T.M., Hansen, S.G., Nelson, J.A., and
768 Fruh, K.J. (2006). Interferon regulatory factor 3 is necessary for induction of
769 antiviral genes during human cytomegalovirus infection. Journal of virology *80*,
770 1032-1037.

771 Devos, M., Tanghe, G., Gilbert, B., Dierick, E., Verheirstraeten, M., Nemegeer,
772 J., de Reuver, R., Lefebvre, S., De Munck, J., Rehwinkel, J.*, et al.* (2020).
773 Sensing of endogenous nucleic acids by ZBP1 induces keratinocyte
774 necroptosis and skin inflammation. The Journal of experimental medicine *217*.

775 Di Tommaso, P., Chatzou, M., Floden, E.W., Barja, P.P., Palumbo, E., and
776 Notredame, C. (2017). Nextflow enables reproducible computational workflows.
777 Nat Biotechnol *35*, 316-319.

778 Dias Junior, A.G., Sampaio, N.G., and Rehwinkel, J. (2019). A Balancing Act:
779 MDA5 in Antiviral Immunity and Autoinflammation. Trends in microbiology *27*,
780 75-85.

781 Dobin, A., Davis, C.A., Schlesinger, F., Drenkow, J., Zaleski, C., Jha, S., Batut,
782 P., Chaisson, M., and Gingeras, T.R. (2013). STAR: ultrafast universal RNA-
783 seq aligner. Bioinformatics *29*, 15-21.

784 Eisenberg, E., and Levanon, E.Y. (2018). A-to-I RNA editing - immune protector
785 and transcriptome diversifier. Nature reviews. Genetics *19*, 473-490.

786 Feng, S., Li, H., Zhao, J., Pervushin, K., Lowenhaupt, K., Schwartz, T.U., and

787 Droge, P. (2011). Alternate rRNA secondary structures as regulators of
788 translation. Nature structural & molecular biology *18*, 169-176.

789 Gannon, H.S., Zou, T., Kiessling, M.K., Gao, G.F., Cai, D., Choi, P.S., Ivan, A.P.,
790 Buchumenski, I., Berger, A.C., Goldstein, J.T.*, et al.* (2018). Identification of
791 ADAR1 adenosine deaminase dependency in a subset of cancer cells. Nature
792 communications *9*, 5450.

793 Gel, B., Diez-Villanueva, A., Serra, E., Buschbeck, M., Peinado, M.A., and
794 Malinverni, R. (2016). regioneR: an R/Bioconductor package for the association
795 analysis of genomic regions based on permutation tests. Bioinformatics *32*,
796 289-291.

797 Goubau, D., Romieu-Mourez, R., Solis, M., Hernandez, E., Mesplede, T., Lin,
798 R., Leaman, D., and Hiscott, J. (2009). Transcriptional re-programming of
799 primary macrophages reveals distinct apoptotic and anti-tumoral functions of
800 IRF-3 and IRF-7. Eur J Immunol *39*, 527-540.

801 Grandvaux, N., Servant, M.J., tenOever, B., Sen, G.C., Balachandran, S.,
802 Barber, G.N., Lin, R., and Hiscott, J. (2002). Transcriptional profiling of
803 interferon regulatory factor 3 target genes: direct involvement in the regulation
804 of interferon-stimulated genes. Journal of virology *76*, 5532-5539.

805 Guallar, D., Fuentes-Iglesias, A., Souto, Y., Ameneiro, C., Freire-Agulleiro, O.,
806 Pardavila, J.A., Escudero, A., Garcia-Outeiral, V., Moreira, T., Saenz, C.*, et al.*
807 (2020). ADAR1-Dependent RNA Editing Promotes MET and iPSC
808 Reprogramming by Alleviating ER Stress. Cell stem cell *27*, 300-314 e311.

809 Hall, K., Cruz, P., Tinoco, I., Jr., Jovin, T.M., and van de Sande, J.H. (1984). 'Z-
810 RNA'--a left-handed RNA double helix. Nature *311*, 584-586.

811 Harding, H.P., Zhang, Y., Zeng, H., Novoa, I., Lu, P.D., Calfon, M., Sadri, N.,
812 Yun, C., Popko, B., Paules, R.*, et al.* (2003). An integrated stress response
813 regulates amino acid metabolism and resistance to oxidative stress. Molecular
814 cell *11*, 619-633.

815 Hartner, J.C., Schmittwolf, C., Kispert, A., Muller, A.M., Higuchi, M., and
816 Seeburg, P.H. (2004). Liver disintegration in the mouse embryo caused by
817 deficiency in the RNA-editing enzyme ADAR1. J Biol Chem *279*, 4894-4902.

818 Hartner, J.C., Walkley, C.R., Lu, J., and Orkin, S.H. (2009). ADAR1 is essential
819 for the maintenance of hematopoiesis and suppression of interferon signaling.
820 Nature immunology *10*, 109-115.

821 Heraud-Farlow, J.E., and Walkley, C.R. (2020). What do editors do?

822 Understanding the physiological functions of A-to-I RNA editing by adenosine
823 deaminase acting on RNAs. Open Biol *10*, 200085.

824 Herbert, A. (2019). Z-DNA and Z-RNA in human disease. Commun Biol *2*, 7.

825 Ho, P.S., Ellison, M.J., Quigley, G.J., and Rich, A. (1986). A computer aided
826 thermodynamic approach for predicting the formation of Z-DNA in naturally
827 occurring sequences. The EMBO journal *5*, 2737-2744.

828 Ishizuka, J.J., Manguso, R.T., Cheruiyot, C.K., Bi, K., Panda, A., Iracheta-Vellve,
829 A., Miller, B.C., Du, P.P., Yates, K.B., Dubrot, J.*, et al.* (2019). Loss of ADAR1
830 in tumours overcomes resistance to immune checkpoint blockade. Nature *565*,
831 43-48.

832 Jiao, H., Wachsmuth, L., Kumari, S., Schwarzer, R., Lin, J., Eren, R.O., Fisher,
833 A., Lane, R., Young, G.R., Kassiotis, G.*, et al.* (2020). Z-nucleic-acid sensing
834 triggers ZBP1-dependent necroptosis and inflammation. Nature *580*, 391-395.

835 Kesavardhana, S., and Kanneganti, T.D. (2020). ZBP1: A STARGTE to decode
836 the biology of Z-nucleic acids in disease. The Journal of experimental medicine
837 *217*.

838 Kim, D., Paggi, J.M., Park, C., Bennett, C., and Salzberg, S.L. (2019). Graph-
839 based genome alignment and genotyping with HISAT2 and HISAT-genotype.
840 Nat Biotechnol *37*, 907-915.

841 Kim, S.H., Lim, S.H., Lee, A.R., Kwon, D.H., Song, H.K., Lee, J.H., Cho, M.,
842 Johner, A., Lee, N.K., and Hong, S.C. (2018). Unveiling the pathway to Z-DNA
843 in the protein-induced B-Z transition. Nucleic acids research *46*, 4129-4137.

844 Kim, Y.G., Muralinath, M., Brandt, T., Pearcy, M., Hauns, K., Lowenhaupt, K.,
845 Jacobs, B.L., and Rich, A. (2003). A role for Z-DNA binding in vaccinia virus
846 pathogenesis. Proceedings of the National Academy of Sciences of the United
847 States of America *100*, 6974-6979.

848 Lazear, H.M., Lancaster, A., Wilkins, C., Suthar, M.S., Huang, A., Vick, S.C.,
849 Clepper, L., Thackray, L., Brassil, M.M., Virgin, H.W.*, et al.* (2013). IRF-3, IRF-
850 5, and IRF-7 coordinately regulate the type I IFN response in myeloid dendritic
851 cells downstream of MAVS signaling. PLoS Pathog *9*, e1003118.

852 Li, H. (2011). A statistical framework for SNP calling, mutation discovery,
853 association mapping and population genetical parameter estimation from
854 sequencing data. Bioinformatics *27*, 2987-2993.

855 Li, H., Xiao, J., Li, J., Lu, L., Feng, S., and Droge, P. (2009). Human genomic

Z-DNA segments probed by the Z alpha domain of ADAR1. Nucleic acids research *37*, 2737-2746.

Li, X.D., Wu, J., Gao, D., Wang, H., Sun, L., and Chen, Z.J. (2013). Pivotal roles of cGAS-cGAMP signaling in antiviral defense and immune adjuvant effects. Science *341*, 1390-1394.

Li, Y., Banerjee, S., Goldstein, S.A., Dong, B., Gaughan, C., Rath, S., Donovan, J., Korennykh, A., Silverman, R.H., and Weiss, S.R. (2017). Ribonuclease L mediates the cell-lethal phenotype of double-stranded RNA editing enzyme ADAR1 deficiency in a human cell line. Elife *6*.

Li, Z., Wolff, K.C., and Samuel, C.E. (2010). RNA adenosine deaminase ADAR1 deficiency leads to increased activation of protein kinase PKR and reduced vesicular stomatitis virus growth following interferon treatment. Virology *396*, 316-322.

Liao, Y., Smyth, G.K., and Shi, W. (2014). featureCounts: an efficient general purpose program for assigning sequence reads to genomic features. Bioinformatics *30*, 923-930.

Liddicoat, B.J., Piskol, R., Chalk, A.M., Ramaswami, G., Higuchi, M., Hartner, J.C., Li, J.B., Seeburg, P.H., and Walkley, C.R. (2015). RNA editing by ADAR1 prevents MDA5 sensing of endogenous dsRNA as nonself. Science *349*, 1115-1120.

Liu, H., Golji, J., Brodeur, L.K., Chung, F.S., Chen, J.T., deBeaumont, R.S., Bullock, C.P., Jones, M.D., Kerr, G., Li, L.*, et al.* (2019). Tumor-derived IFN triggers chronic pathway agonism and sensitivity to ADAR loss. Nature medicine *25*, 95-102.

Love, M.I., Huber, W., and Anders, S. (2014). Moderated estimation of fold change and dispersion for RNA-seq data with DESeq2. Genome Biol *15*, 550.

Luo, H., Wang, D., Che, H.L., Zhao, Y., and Jin, H. (2012). Pathological observations of lung inflammation after administration of IP-10 in influenza virus- and respiratory syncytial virus-infected mice. Exp Ther Med *3*, 76-79.

Maelfait, J., Liverpool, L., Bridgeman, A., Ragan, K.B., Upton, J.W., and Rehwinkel, J. (2017). Sensing of viral and endogenous RNA by ZBP1/DAI induces necroptosis. The EMBO journal *36*, 2529-2543.

Maelfait, J., Liverpool, L., and Rehwinkel, J. (2020). Nucleic Acid Sensors and Programmed Cell Death. Journal of molecular biology *432*, 552-568.

Mannion, N.M., Greenwood, S.M., Young, R., Cox, S., Brindle, J., Read, D., Nellaker, C., Vesely, C., Ponting, C.P., McLaughlin, P.J., *et al.* (2014). The RNA-editing enzyme ADAR1 controls innate immune responses to RNA. Cell reports *9*, 1482-1494.

Martin, M. (2011). Cutadapt removes adapter sequences from high-throughput sequencing reads. 2011 *17*, 3.

Mehdipour, P., Marhon, S.A., Ettayebi, I., Chakravarthy, A., Hosseini, A., Wang, Y., de Castro, F.A., Loo Yau, H., Ishak, C., Abelson, S., *et al.* (2020). Epigenetic therapy induces transcription of inverted SINEs and ADAR1 dependency. Nature *588*, 169-173.

Michallet, M.C., Meylan, E., Ermolaeva, M.A., Vazquez, J., Rebsamen, M., Curran, J., Poeck, H., Bscheider, M., Hartmann, G., Konig, M., *et al.* (2008). TRADD protein is an essential component of the RIG-like helicase antiviral pathway. Immunity *28*, 651-661.

Pakos-Zebrucka, K., Koryga, I., Mnich, K., Ljujic, M., Samali, A., and Gorman, A.M. (2016). The integrated stress response. EMBO reports *17*, 1374-1395.

Perng, Y.C., and Lenschow, D.J. (2018). ISG15 in antiviral immunity and beyond. Nature reviews. Microbiology *16*, 423-439.

Pestal, K., Funk, C.C., Snyder, J.M., Price, N.D., Treuting, P.M., and Stetson, D.B. (2015). Isoforms of RNA-Editing Enzyme ADAR1 Independently Control Nucleic Acid Sensor MDA5-Driven Autoimmunity and Multi-organ Development. Immunity *43*, 933-944.

Pfaller, C.K., Donohue, R.C., Nersisyan, S., Brodsky, L., and Cattaneo, R. (2018). Extensive editing of cellular and viral double-stranded RNA structures accounts for innate immunity suppression and the proviral activity of ADAR1p150. PLoS Biol *16*, e2006577.

Pichlmair, A., Lassnig, C., Eberle, C.A., Gorna, M.W., Baumann, C.L., Burkard, T.R., Burckstummer, T., Stefanovic, A., Krieger, S., Bennett, K.L., *et al.* (2011). IFIT1 is an antiviral protein that recognizes 5'-triphosphate RNA. Nature immunology *12*, 624-630.

Piechotta, M., and Dieterich, C. (2013). ACCUSA2: multi-purpose SNV calling enhanced by probabilistic integration of quality scores. Bioinformatics *29*, 1809-1810.

Piechotta, M., Wyler, E., Ohler, U., Landthaler, M., and Dieterich, C. (2017). JACUSA: site-specific identification of RNA editing events from replicate

925 sequencing data. BMC Bioinformatics *18*, 7.

926 Porath, H.T., Knisbacher, B.A., Eisenberg, E., and Levanon, E.Y. (2017).
927 Massive A-to-I RNA editing is common across the Metazoa and correlates with
928 dsRNA abundance. Genome Biol *18*, 185.

929 Quinlan, A.R., and Hall, I.M. (2010). BEDTools: a flexible suite of utilities for
930 comparing genomic features. Bioinformatics *26*, 841-842.

931 Reich, D.P., and Bass, B.L. (2019). Mapping the dsRNA World. Cold Spring
932 Harb Perspect Biol *11*.

933 Rice, G.I., Kasher, P.R., Forte, G.M., Mannion, N.M., Greenwood, S.M.,
934 Szynkiewicz, M., Dickerson, J.E., Bhaskar, S.S., Zampini, M., Briggs, T.A.*, et*
935 *al.* (2012). Mutations in ADAR1 cause Aicardi-Goutieres syndrome associated
936 with a type I interferon signature. Nature genetics *44*, 1243-1248.

937 Schade, M., Turner, C.J., Lowenhaupt, K., Rich, A., and Herbert, A. (1999).
938 Structure-function analysis of the Z-DNA-binding domain Zalpha of dsRNA
939 adenosine deaminase type I reveals similarity to the (alpha + beta) family of
940 helix-turn-helix proteins. The EMBO journal *18*, 470-479.

941 Schoggins, J.W. (2019). Interferon-Stimulated Genes: What Do They All Do?
942 Annu Rev Virol *6*, 567-584.

943 Schwartz, T., Rould, M.A., Lowenhaupt, K., Herbert, A., and Rich, A. (1999).
944 Crystal structure of the Zalpha domain of the human editing enzyme ADAR1
945 bound to left-handed Z-DNA. Science *284*, 1841-1845.

946 Solomon, O., Di Segni, A., Cesarkas, K., Porath, H.T., Marcu-Malina, V., Mizrahi,
947 O., Stern-Ginossar, N., Kol, N., Farage-Barhom, S., Glick-Saar, E.*, et al.* (2017).
948 RNA editing by ADAR1 leads to context-dependent transcriptome-wide
949 changes in RNA secondary structure. Nature communications *8*, 1440.

950 Song, Y., Yang, W., Fu, Q., Wu, L., Zhao, X., Zhang, Y., and Zhang, R. (2020).
951 irCLASH reveals RNA substrates recognized by human ADARs. Nature
952 structural & molecular biology *27*, 351-362.

953 Sridharan, H., Ragan, K.B., Guo, H., Gilley, R.P., Landsteiner, V.J., Kaiser, W.J.,
954 and Upton, J.W. (2017). Murine cytomegalovirus IE3-dependent transcription
955 is required for DAI/ZBP1-mediated necroptosis. EMBO reports *18*, 1429-1441.

956 Tan, M.H., Li, Q., Shanmugam, R., Piskol, R., Kohler, J., Young, A.N., Liu, K.I.,
957 Zhang, R., Ramaswami, G., Ariyoshi, K.*, et al.* (2017). Dynamic landscape and
958 regulation of RNA editing in mammals. Nature *550*, 249-254.

959 Uggenti, C., Lepelley, A., and Crow, Y.J. (2019). Self-Awareness: Nucleic Acid-
960 Driven Inflammation and the Type I Interferonopathies. Annual review of
961 immunology *37*, 247-267.

962 Vogel, O.A., Han, J., Liang, C.Y., Manicassamy, S., Perez, J.T., and
963 Manicassamy, B. (2020). The p150 Isoform of ADAR1 Blocks Sustained RLR
964 signaling and Apoptosis during Influenza Virus Infection. PLoS Pathog *16*,
965 e1008842.

966 Wang, A.H., Quigley, G.J., Kolpak, F.J., Crawford, J.L., van Boom, J.H., van der
967 Marel, G., and Rich, A. (1979). Molecular structure of a left-handed double
968 helical DNA fragment at atomic resolution. Nature *282*, 680-686.

969 Wang, L., Wang, S., and Li, W. (2012). RSeQC: quality control of RNA-seq
970 experiments. Bioinformatics *28*, 2184-2185.

971 Wang, Q., Miyakoda, M., Yang, W., Khillan, J., Stachura, D.L., Weiss, M.J., and
972 Nishikura, K. (2004). Stress-induced apoptosis associated with null mutation of
973 ADAR1 RNA editing deaminase gene. J Biol Chem *279*, 4952-4961.

974 Wang, R., Li, H., Wu, J., Cai, Z.Y., Li, B., Ni, H., Qiu, X., Chen, H., Liu, W., Yang,
975 Z.H.*, et al.* (2020). Gut stem cell necroptosis by genome instability triggers
976 bowel inflammation. Nature *580*, 386-390.

977 Ward, S.V., George, C.X., Welch, M.J., Liou, L.Y., Hahm, B., Lewicki, H., de la
978 Torre, J.C., Samuel, C.E., and Oldstone, M.B. (2011). RNA editing enzyme
979 adenosine deaminase is a restriction factor for controlling measles virus
980 replication that also is required for embryogenesis. Proceedings of the National
981 Academy of Sciences of the United States of America *108*, 331-336.

982 Weiden, M.D., Hoshino, S., Levy, D.N., Li, Y., Kumar, R., Burke, S.A., Dawson,
983 R., Hioe, C.E., Borkowsky, W., Rom, W.N., and Hoshino, Y. (2014). Adenosine
984 deaminase acting on RNA-1 (ADAR1) inhibits HIV-1 replication in human
985 alveolar macrophages. PloS one *9*, e108476.

986 Wittig, B., Wolfl, S., Dorbic, T., Vahrson, W., and Rich, A. (1992). Transcription
987 of human c-myc in permeabilized nuclei is associated with formation of Z-DNA
988 in three discrete regions of the gene. The EMBO journal *11*, 4653-4663.

989 Wolfl, S., Wittig, B., and Rich, A. (1995). Identification of transcriptionally
990 induced Z-DNA segments in the human c-myc gene. Biochim Biophys Acta
991 *1264*, 294-302.

992 Young, M.D., Wakefield, M.J., Smyth, G.K., and Oshlack, A. (2010). Gene
993 ontology analysis for RNA-seq: accounting for selection bias. Genome Biol *11*,

994 R14.

995 Zhabinskaya, D., and Benham, C.J. (2011). Theoretical analysis of the stress
996 induced B-Z transition in superhelical DNA. PLoS Comput Biol *7*, e1001051.

997 Zhang, H., Ni, G., and Damania, B. (2020a). ADAR1 Facilitates KSHV Lytic
998 Reactivation by Modulating the RLR-Dependent Signaling Pathway. Cell
999 reports *31*, 107564.

1000 Zhang, T., Yin, C., Boyd, D.F., Quarato, G., Ingram, J.P., Shubina, M., Ragan,
1001 K.B., Ishizuka, T., Crawford, J.C., Tummers, B.*, et al.* (2020b). Influenza Virus
1002 Z-RNAs Induce ZBP1-Mediated Necroptosis. Cell *180*, 1115-1129 e1113.

1003 Zhou, S., Yang, C., Zhao, F., Huang, Y., Lin, Y., Huang, C., Ma, X., Du, J., Wang,
1004 Y., Long, G.*, et al.* (2019). Double-stranded RNA deaminase ADAR1 promotes
1005 the Zika virus replication by inhibiting the activation of protein kinase PKR. J
1006 Biol Chem *294*, 18168-18180.
1007

1008 **Figures and figure legends**

1009

1010

Figure 1.

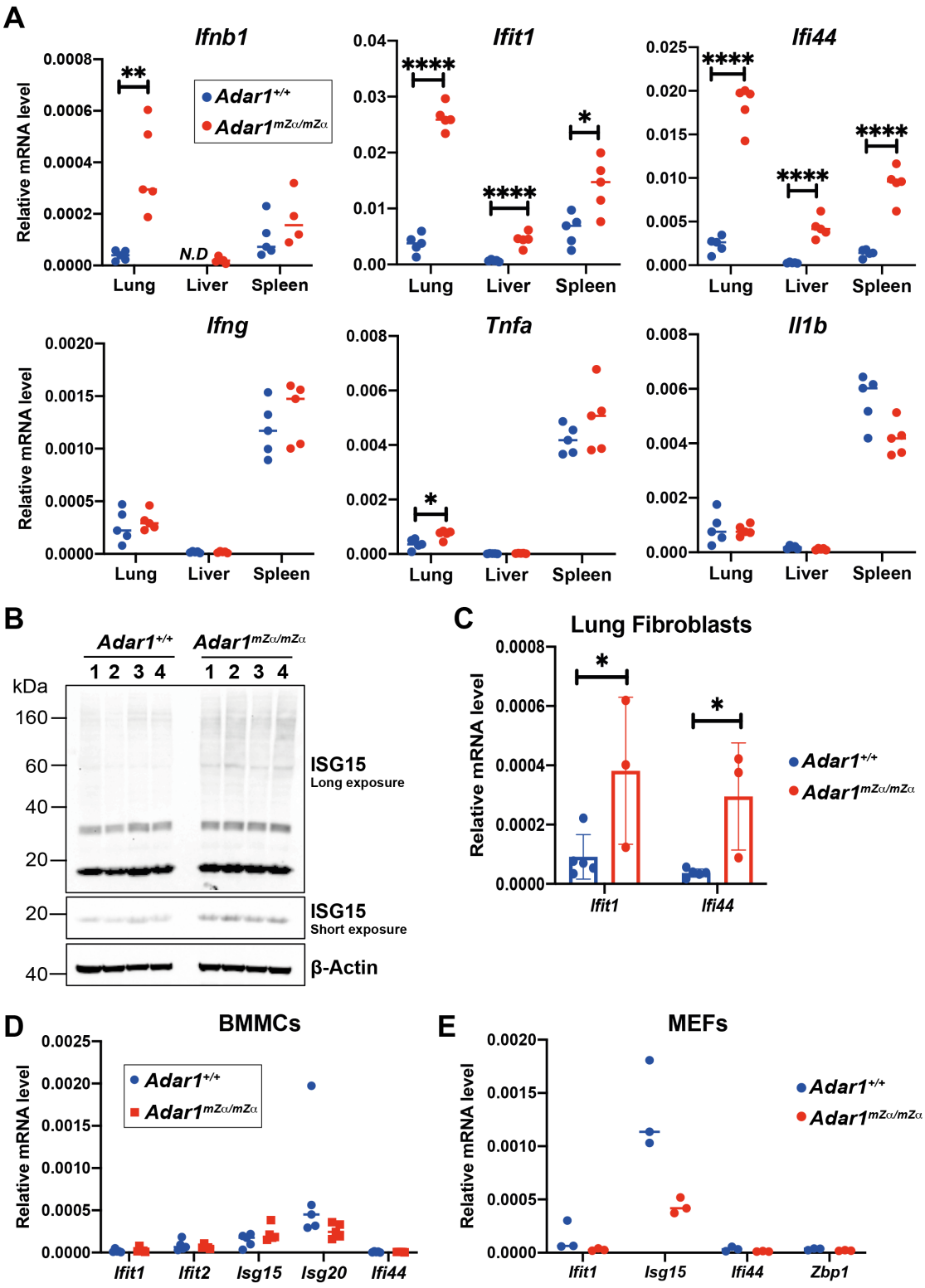

1011

1012

Figure 1. Mutation of ADAR1-p150's Zα domain triggers spontaneous type I IFN responses in multiple organs.

A. Levels of the indicated mRNAs were analysed by RT-qPCR in RNA samples extracted from tissues of WT and *Adar1*$^{mZ\alpha/mZ\alpha}$ animals and are shown relative to *Gapdh*. Each dot represents an individual mouse. *N.D*, not detectable.

B. Protein extracts from whole lungs from animals of the indicated genotypes were used for western blot with an α-ISG15 antibody. β-Actin served as a loading control. Each lane represents a sample from an individual mouse.

C-E. mRNA levels of the indicated ISGs were analysed by RT-qPCR from cultured lung fibroblasts (C), BMMCs (D), and MEFs (E) of the indicated genotypes and are shown relative to *Gapdh*. Each dot represents cells derived from an individual mouse.

Pooled data from biological replicates are shown with mean (A, D, E) or mean ± SD (C) and were analysed by unpaired t test (****p<0.0001, **p<0.01, *p<0.05). See also Figure S1.

Figure S1.

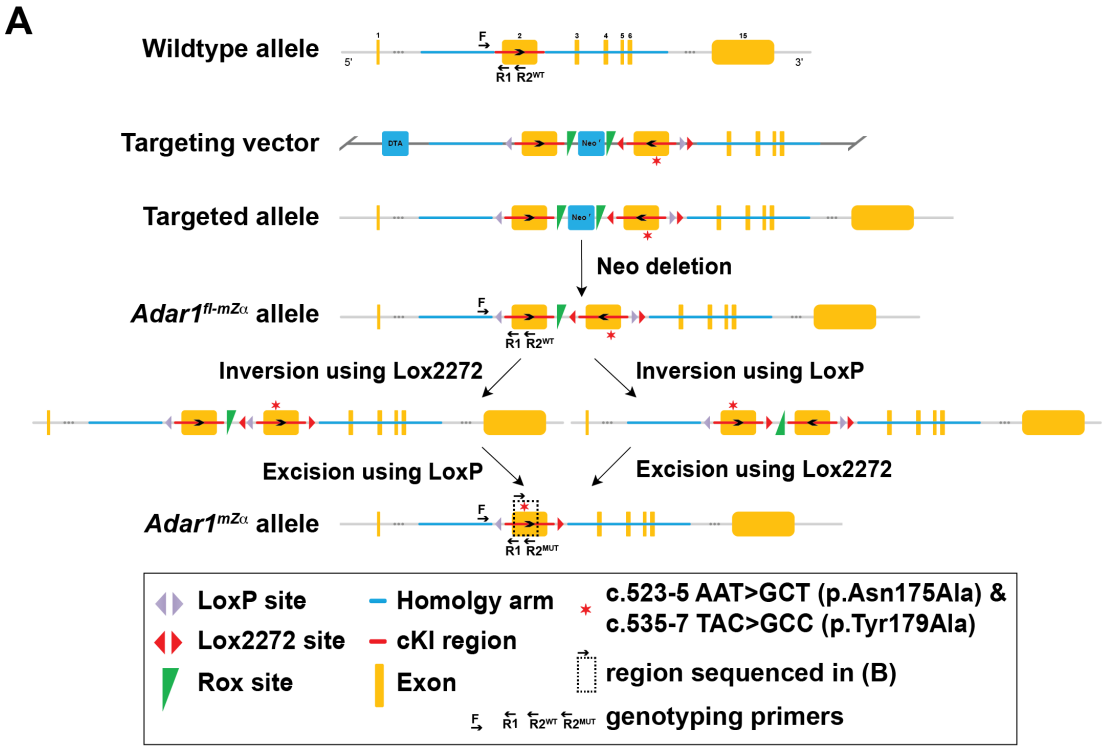

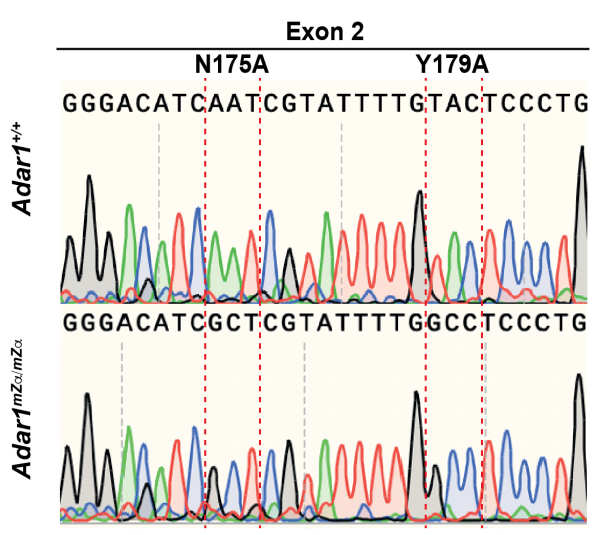

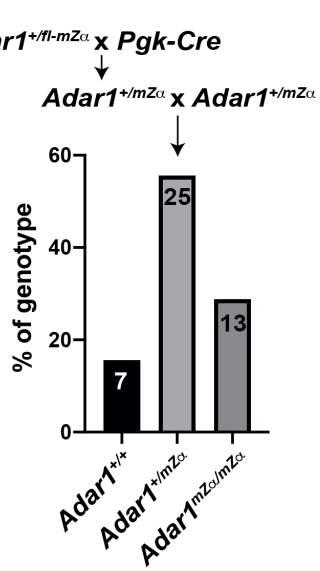

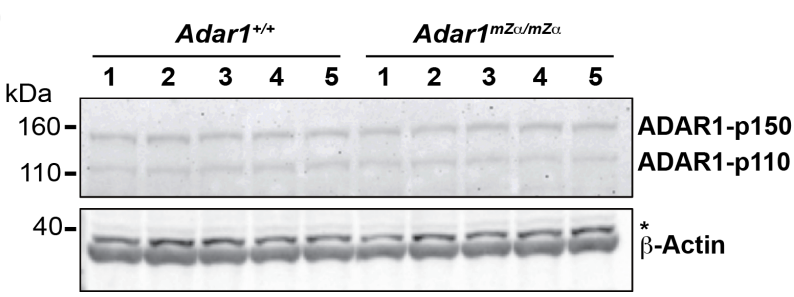

Figure S1, related to Figure1. Generation of *Adar1*$^{mZ\alpha/mZ\alpha}$ animals.

A. Schematic representation of the *Adar1* WT allele, targeting vector, targeted allele, *Adar1*$^{fl\text{-}mZ\alpha}$ allele and the two-step Cre-mediated recombination process that resulted in the *Adar1*$^{mZ\alpha}$ allele. Please see text for details. cKI, conditional knock-in.

B. Genomic DNA was prepared from WT and *Adar1*$^{mZ\alpha/mZ\alpha}$ animals and the mutated region in exon 2 was sequenced.

C. *Adar1*$^{+/fl\text{-}mZ\alpha}$ mice were bred with the *Pgk-Cre* line. *Adar*$^{+/mZ\alpha}$ offspring were then mated to generate *Adar1*$^{mZ\alpha/mZ\alpha}$ animals. The numbers and percentages of animals obtained with the indicated genotypes are shown.

D. BMMCs were grown from bone marrow from five mice of the indicated genotypes. Protein extracts were used for western blot with α-ADAR1 antibody. β-Actin served as a loading control. *, non-specific band

Figure 2.

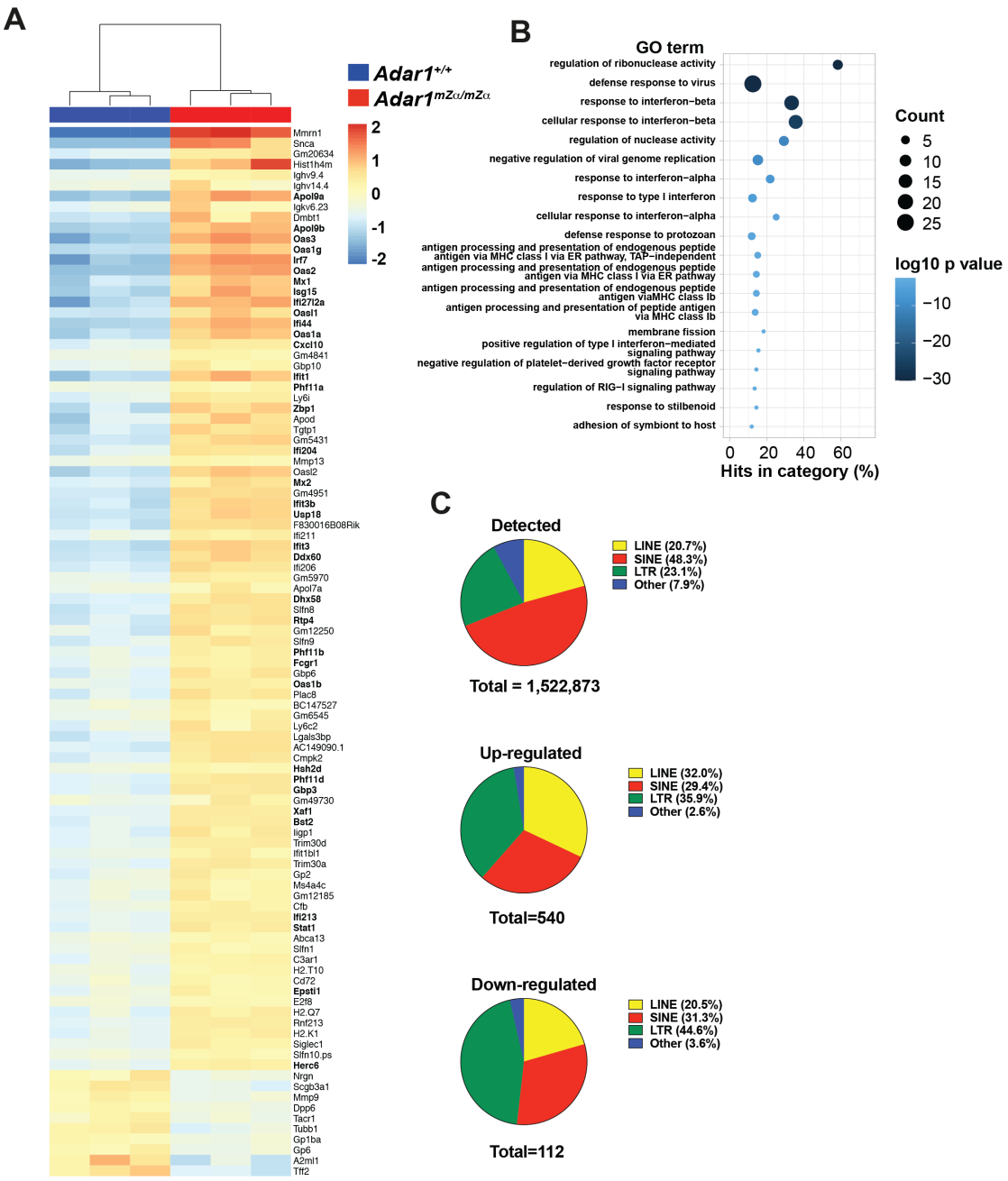

Figure 2. *Adar1*$^{mZ\alpha/mZ\alpha}$ lungs display a type I IFN gene signature.

Total RNA was extracted from lungs of three WT and three *Adar1*$^{mZ\alpha/mZ\alpha}$ mice. Ribosomal RNAs were depleted before random-primed library preparation and RNA sequencing. About 100 million reads were obtained per sample.

A. Differentially expressed genes were defined as displaying a fold change of ≥2 with an adjusted p-value <0.01. The 89 upregulated and 10 downregulated

genes were ordered by decreasing fold change and the data were clustered by sample. ISGs are indicated in bold.

B. GO analysis of up-regulated genes. The top 20 GO terms (biological processes), ranked and ordered by p-value, are shown. Diameters indicate the number of induced genes assigned to the GO term and colours show the p-value.

C. Detected and differentially expressed REs were assigned to the indicated classes and are shown as pie charts. Differentially expressed REs were identified as having a minimum fold change of 2 and an adjusted p value of less than 0.01.

See also Table S1.

Figure 3.

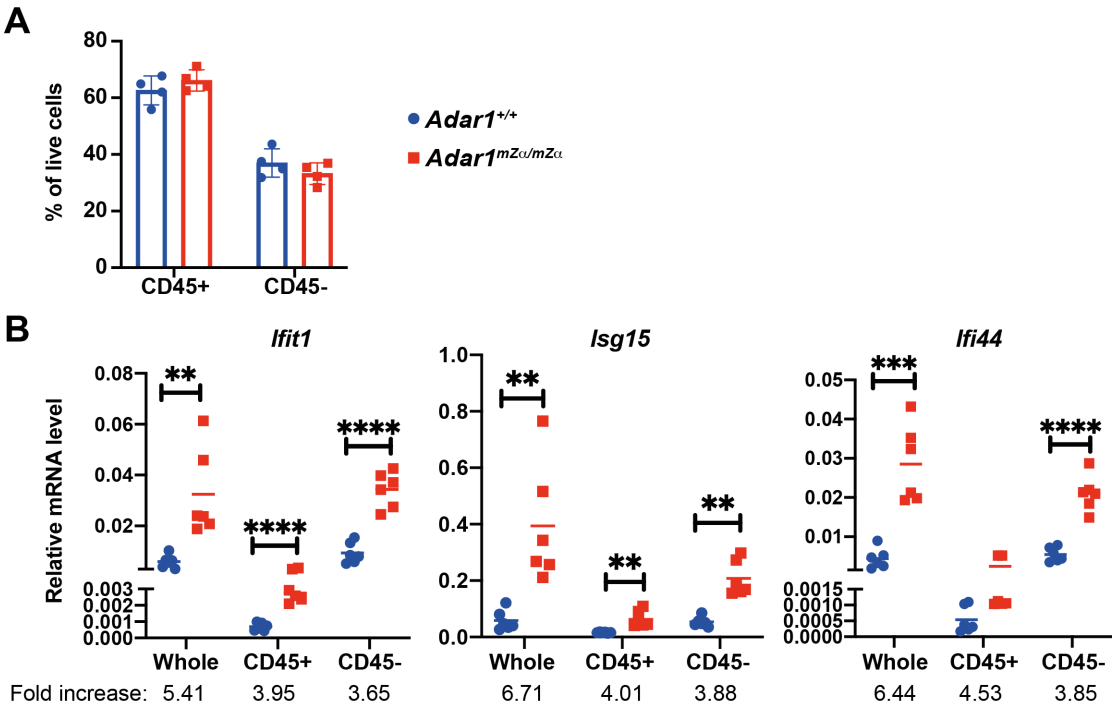

Figure 3. Stromal and haematopoietic cells upregulate ISGs in *Adar1*$^{mZ\alpha/mZ\alpha}$ lungs.

A. The proportion of haematopoietic (CD45+) and stromal (CD45-) cells in WT and *Adar1*$^{mZ\alpha/mZ\alpha}$ lungs is shown.

B. mRNA levels of the indicated ISGs were analysed by RT-qPCR using RNA extracted from whole lung, or from CD45+ or CD45- cells, and are shown relative to *Actb*. Fold increases relative to WT samples were calculated.

Data points represent individual animals. In (A), data from a representative experiment are shown with mean ± SD. In (B), pooled data from two independent experiments including a total of six animals are shown with mean and were analysed by unpaired t test (****p < 0.0001, ***p<0.001, **p<0.01). See also Figure S2.

Figure S2.

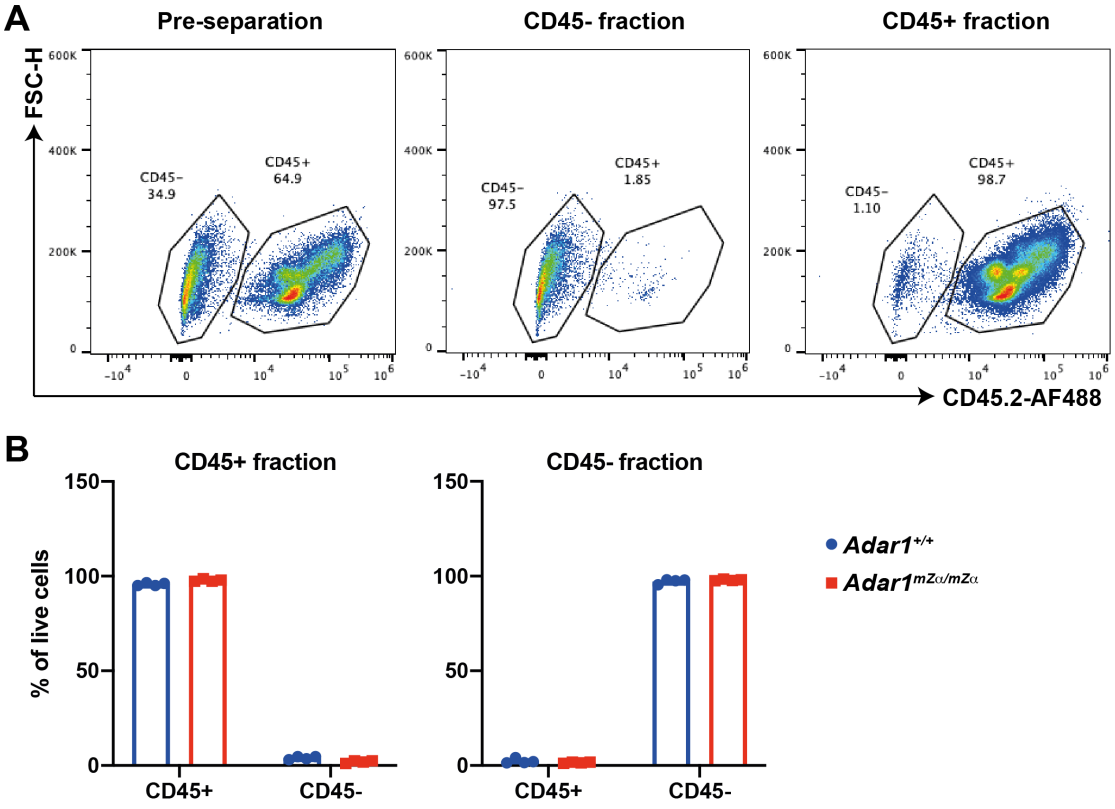

Figure S2, related to Figure 3. MACS separation of lung cells.

A. Cell surface levels of CD45 were analysed by flow cytometry in single cell suspensions obtained from lung tissue before MACS (left) and in CD45- and CD45+ cell fractions obtained after MACS (middle and right). Data are from a representative WT animal.

B. The percentage of CD45-expressing cells is shown for CD45+ and CD45- MACS fractions. Data points represent individual animals (n=4) from a representative experiment and bars indicate the mean.

Figure 4.

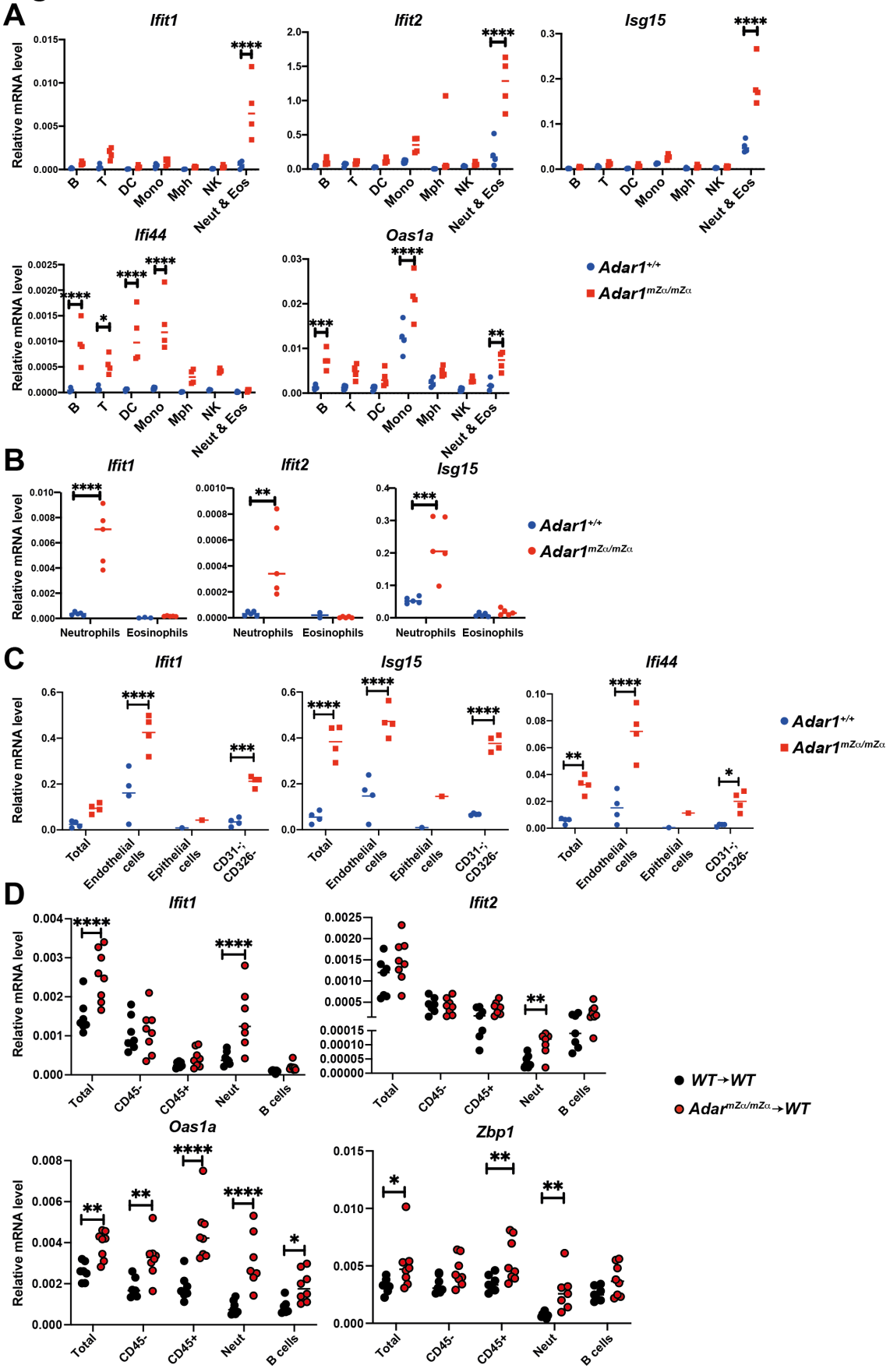

1087

1088 Figure 4. Multiple haematopoietic and non-haematopoietic cell types display
1089 ISGs upregulation in *Adar1*$^{mZ\alpha/mZ\alpha}$ lungs.

1090 **A-C.** mRNA levels of the indicated ISGs were analysed by RT-qPCR using RNA
1091 extracted from cell populations sorted from lungs of WT and *Adar1*$^{mZ\alpha/mZ\alpha}$ mice
1092 and are shown relative to *Actb*. B, B cells; T, T cells; DC, dendritic cells; Mono,
1093 monocytes; Mph, macrophages; NK, natural killer cells; Neut, neutrophils; Eos,
1094 eosinophils; Total, whole lung.

1095 **D.** ISG mRNA levels were analysed as in (A-C) in cell populations sorted from
1096 lungs of BM chimeric mice and are shown relative to *Gapdh*.

1097 Each data point represents an individual mouse. Due to the small number of
1098 epithelial cells recovered, samples were pooled from multiple mice before RNA
1099 extraction (C). Pooled data from two (A,B) or three (D) independent
1100 experiments are shown with mean (****p < 0.0001, ***p<0.001, **p<0.01,
1101 *p<0.05, unpaired t test). See also Figures S3, S4 and S5.

Figure S3.

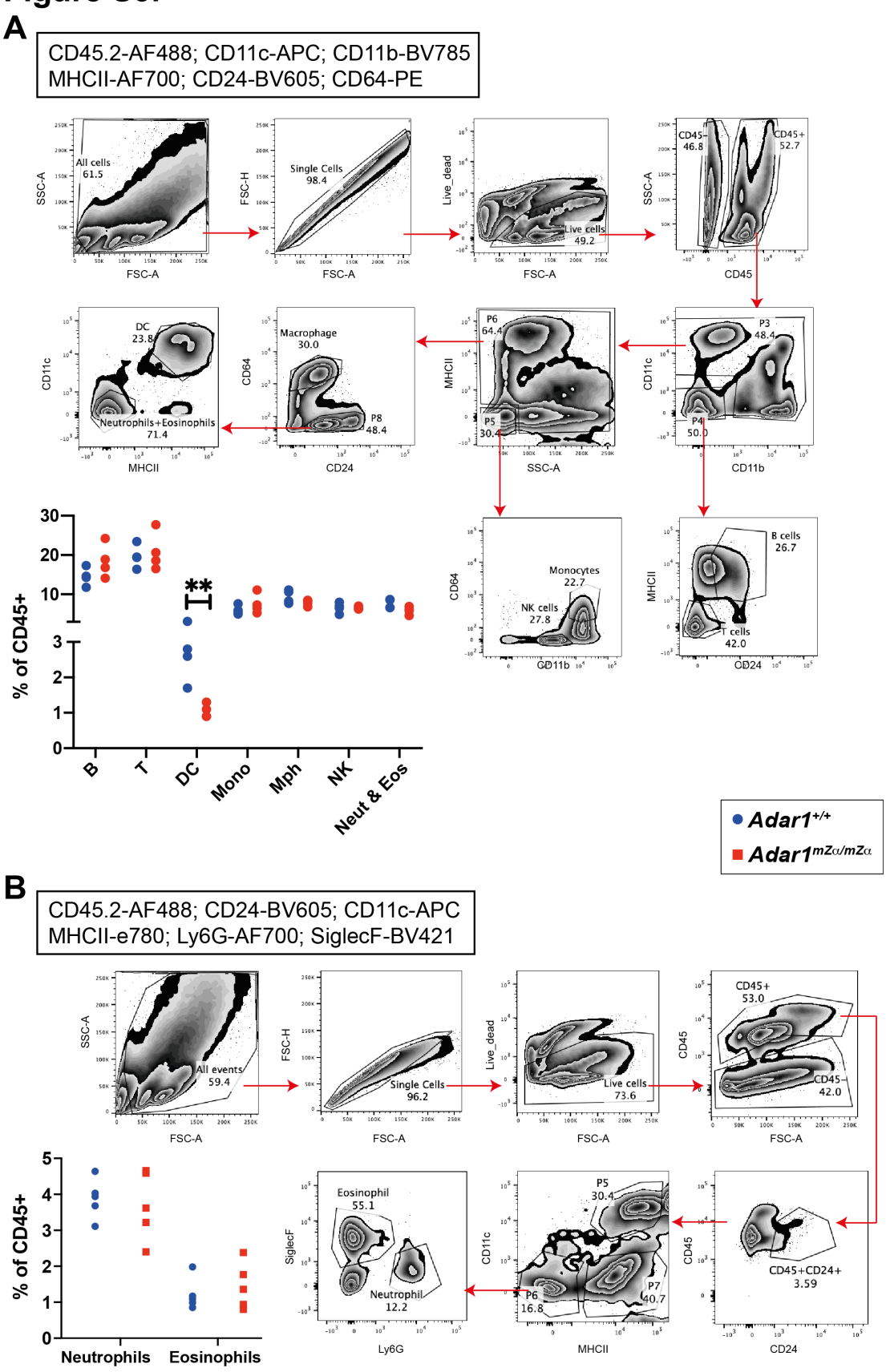

1102

Figure S3, related to Figure 4A and 4B. Gating strategy for sorting of haematopoietic lung cells.

Two staining panels were used to identify and isolate haematopoietic cell populations by FACS. Panel (A) is related to Figure 4A and panel (B) to Figure 4B. Antibodies and conjugated fluorophores are shown in boxes. Gating strategies are shown for a representative WT (A) and *Adar1*$^{mZ\alpha/mZ\alpha}$ (B) animal. Bar graphs show the proportion of each cell population as a percentage of CD45+ cells. Each dot represents an individual mouse and data from two independent experiments were pooled (**p<0.01, unpaired t test).

Figure S4.

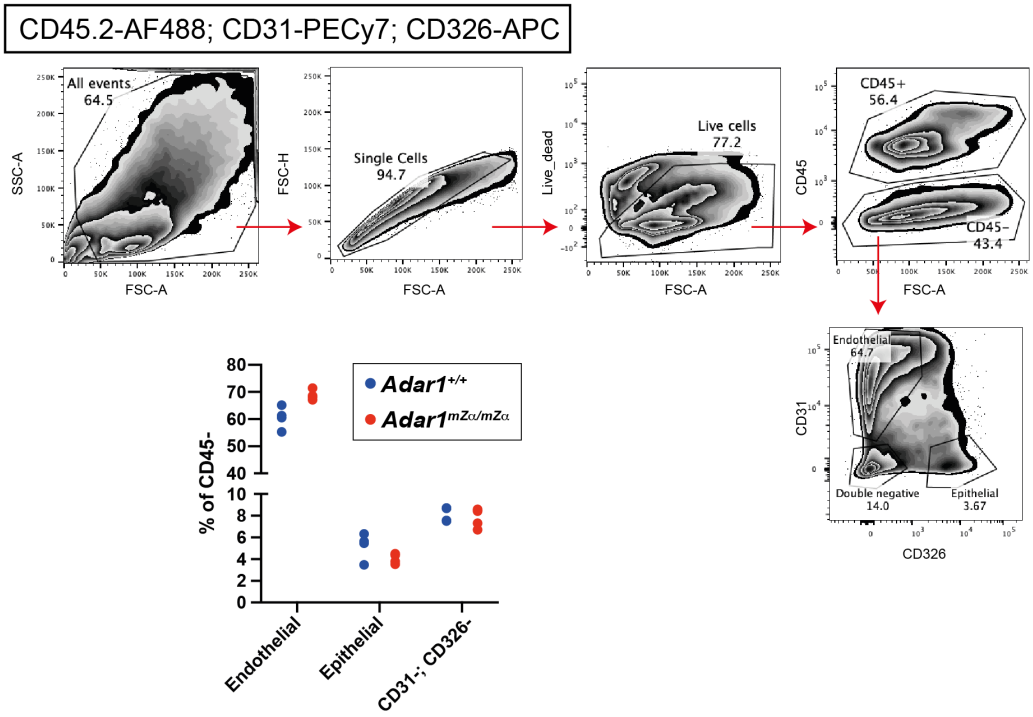

Figure S4, related to Figure 4C. Gating strategy for sorting of stromal lung cells. The staining panel used to identify and isolate non-haematopoietic cell populations by FACS is shown. Antibodies and conjugated fluorophores are shown in the box. The gating strategy is shown for a representative WT animal. The bar graph shows the proportion of each cell population as a percentage of CD45- cells. Each dot represents an individual mouse.

Figure S5.

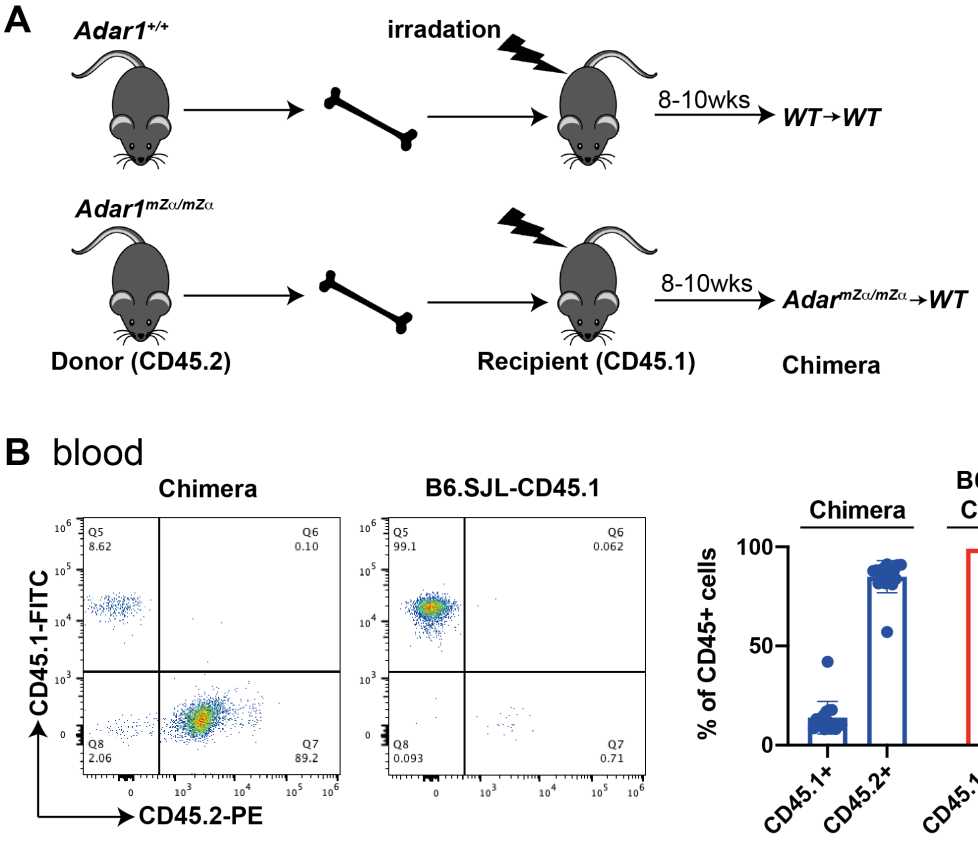

Figure S5, related to Figure 4D. Analysis of BM chimeras.

A. Schematic representation of the generation of BM chimeric animals.

B. White blood cells from BM chimeric mice and, as control, from an untreated B6.SJL-CD45.1 animal, were analysed by FACS. Cells were gated on single, live cells. Representative FACS plots from a WT→WT animal (left) and pooled data from two independent experiments involving a total seven WT→WT and eight *Adar1*$^{mZ\alpha/mZ\alpha}$→WT BM chimeric animals (right) are shown. Bars show the mean and error bars represent SD.

C. Lung cells from BM chimeric mice were analysed by FACS. Data from a representative WT→WT animal are shown.

Figure 5.

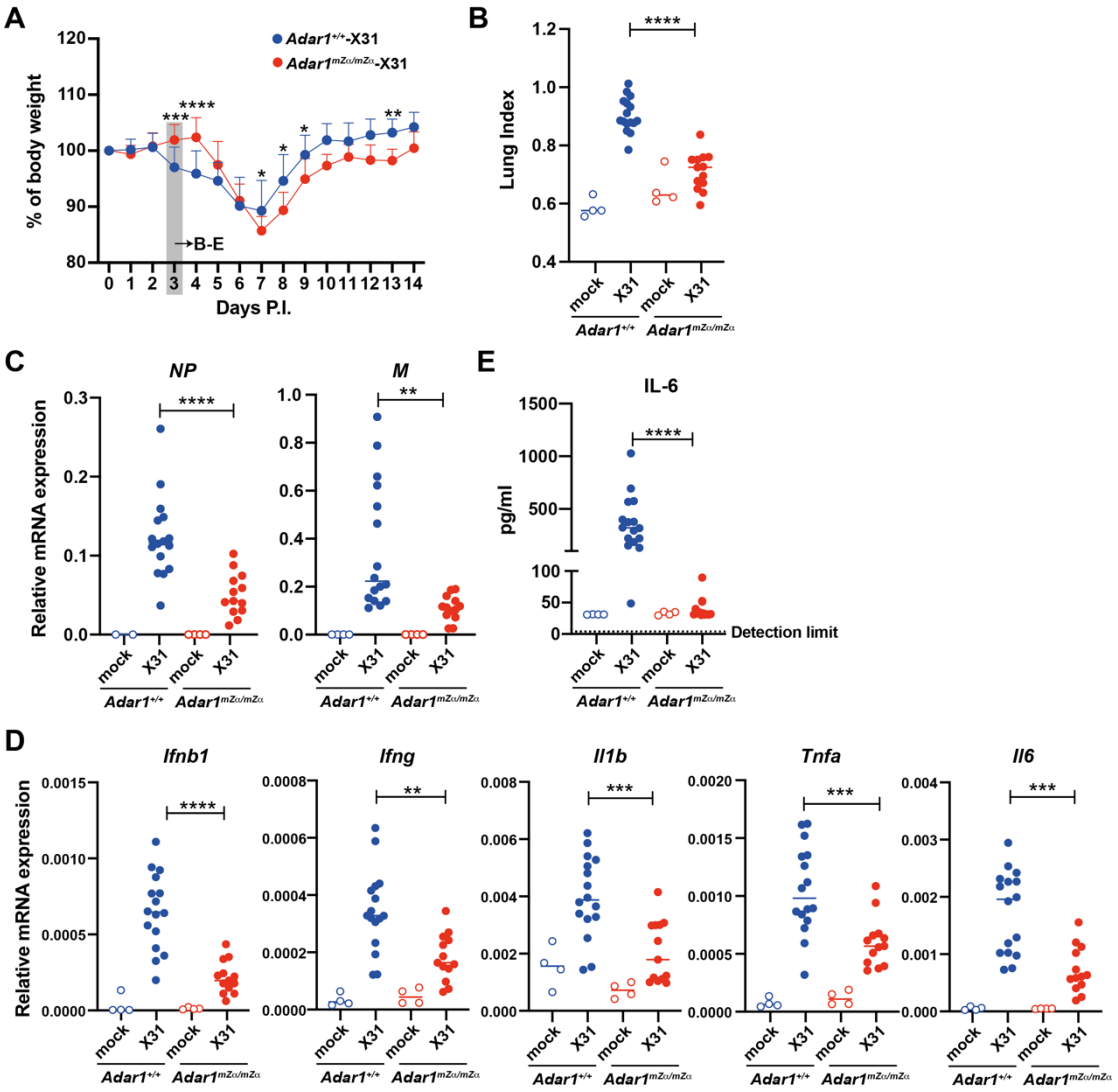

Figure 5. *Adar1*$^{mZ\alpha/mZ\alpha}$ mice are protected from early IAV infection.

A. WT or *Adar1*$^{mZ\alpha/mZ\alpha}$ mice were infected intranasally with 0.04 HAU of IAV strain A/X31. Body weight was monitored daily and is shown as a percentage of starting body weight.

B-E. WT or *Adar1*$^{mZ\alpha/mZ\alpha}$ mice were infected as in (A) or mock infected using viral growth medium. On day 3 post infection, lungs and sera were collected.

B. A 'lung index' was calculated (lung weight/body weight x100).

C. Levels of the viral *NP* and *M* transcripts were analysed by RT-qPCR in RNA samples extracted from total lung. Data are shown relative to *Actb* (*NP*) or *Gapdh* (*M*).

D. Levels of the indicated mRNAs were determined as in (C).

E. Serum IL-6 concentrations were analysed by ELISA.

In (A), data from three independent experiments including a total of 15 mice per genotype were pooled (mean + SD; ****p<0.0001, ***p<0.001, **p<0.01, *p<0.05, mixed-effects analysis). In (B-E), pooled data from two independent experiments (mock infected: n=4 mice per genotype; X31-infected: n=16 WT and n=13 *Adar1*$^{mZ\alpha/mZ\alpha}$ mice) are shown. Each dot represents an individual mouse and the mean is indicated (****p < 0.0001, ***p<0.001, **p<0.01, unpaired t test).

Figure 6.

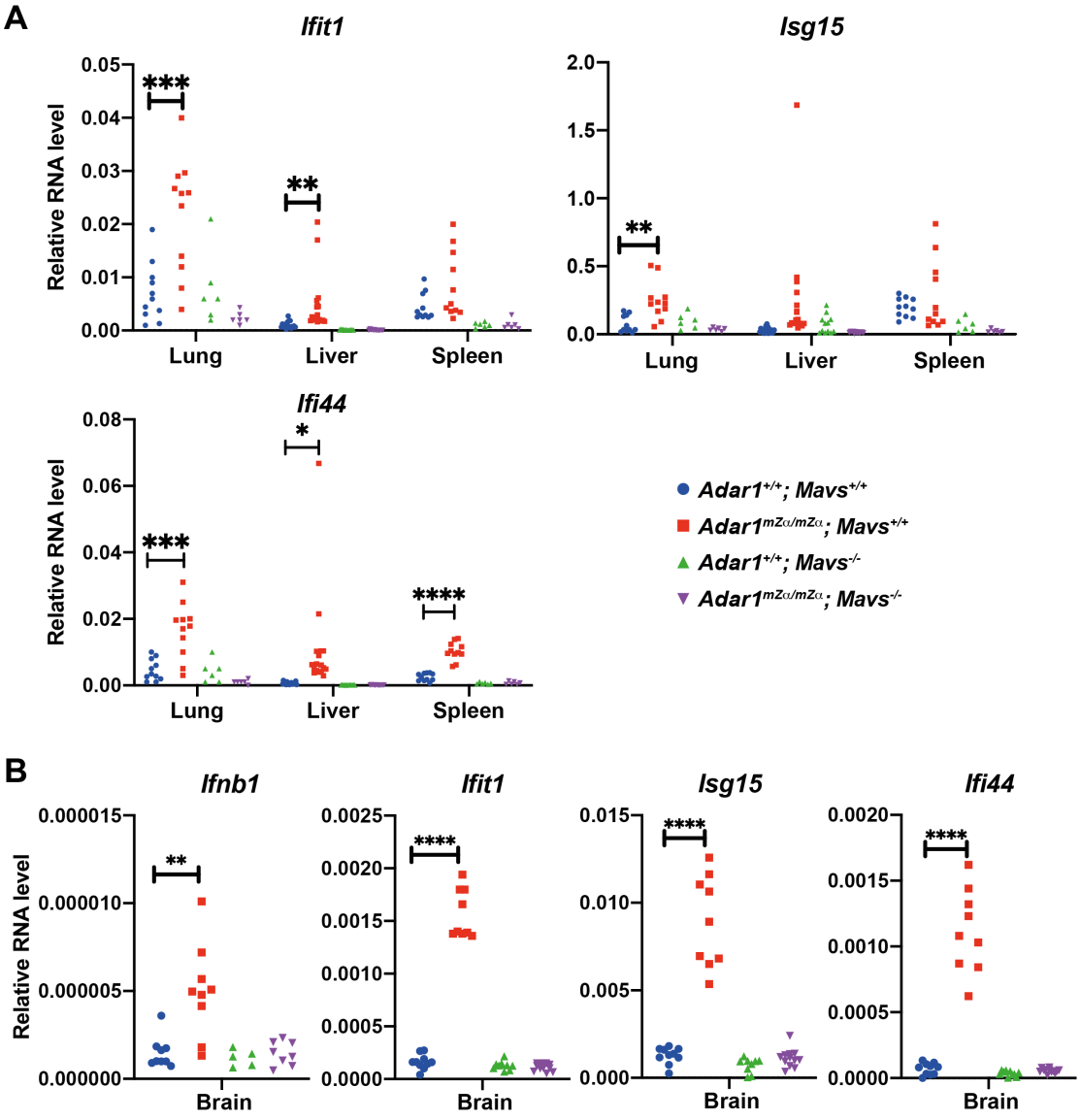

Figure 6. ISG induction in *Adar1*$^{mZ\alpha/mZ\alpha}$ mice is MAVS-dependent.

Levels of the indicated mRNAs were analysed by RT-qPCR in RNA samples extracted from tissues of WT and *Adar1*$^{mZ\alpha/mZ\alpha}$ animals that were either MAVS-sufficient or -deficient. Data are shown relative to *Gapdh*.

Each dot represents an individual mouse. Pooled data from biological replicates are shown (****p < 0.0001, ***p<0.001, **p<0.01, *p<0.05, unpaired t test).

Figure 7.

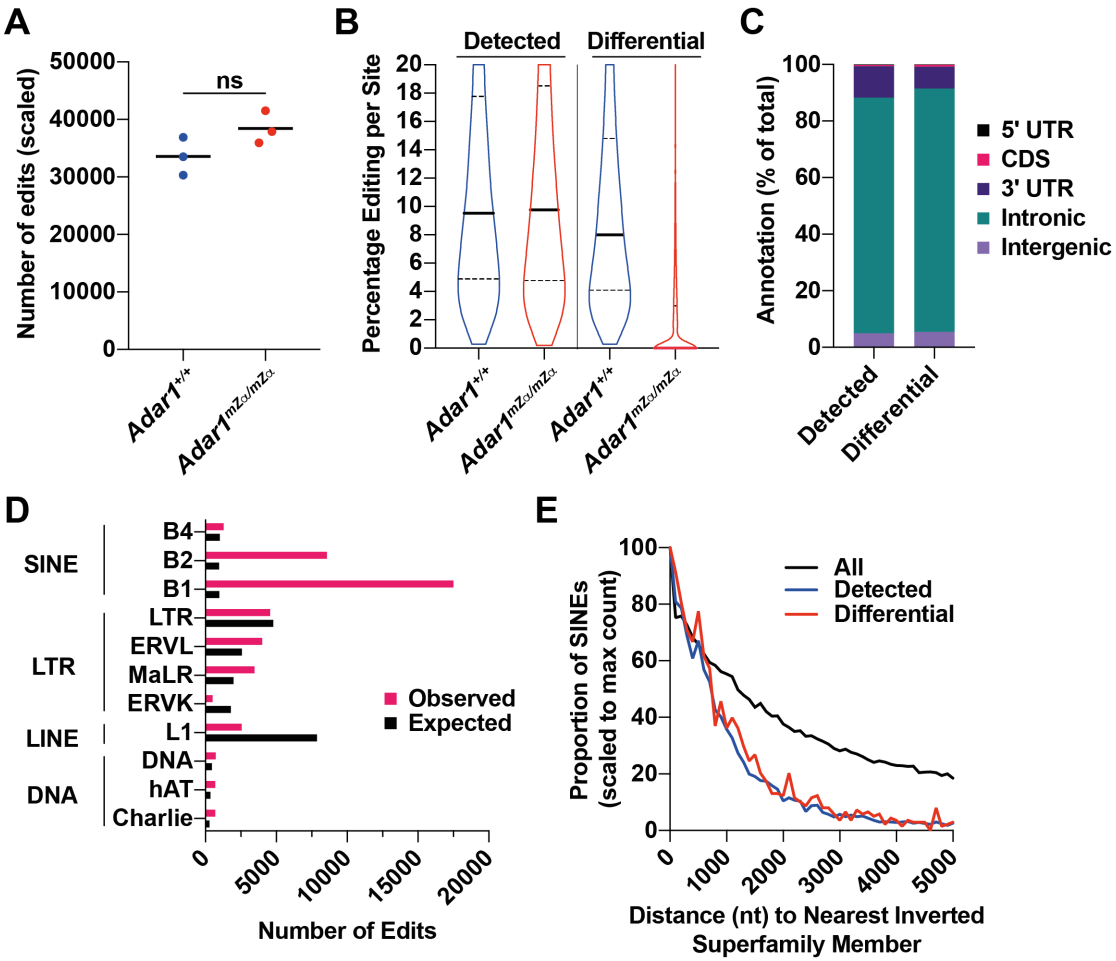

Figure 7. ADAR1-p150's Zα domain is required for editing of a subset of RNAs.

A. Editing sites were mapped in RNA sequencing reads from three WT and three *Adar1*$^{mZ\alpha/mZ\alpha}$ lung samples (Z>2.58). The numbers of edited sites were scaled to the total number of reads per sample. Each data point corresponds to an animal and the mean is shown (ns, not significant; unpaired t test).

B. Editing frequencies for sites detectable in all three WT or *Adar1*$^{mZ\alpha/mZ\alpha}$ samples (left; Z>2.58) and for differentially edited sites (right; Z>2.58, >2-fold) are shown as violin plots. Solid horizontal lines show the median and dotted lines indicate quartiles.

C. Editing sites detected in WT samples and differentially edited sites were matched to annotated genomic features. The percentage of sites is shown for each category.

D. The number of expected and observed editing sites in WT samples are shown for families of REs for which either value exceeded 500. Please see text for details.

E. The distances of SINEs to their nearest inverted super-family member were determined for all SINEs and for SINEs harbouring an editing site in WT samples (Detected) or containing a differentially edited site. Results are shown as proportions of SINEs with the maximum count set to 100.

See also Figure S6.

Figure S6.

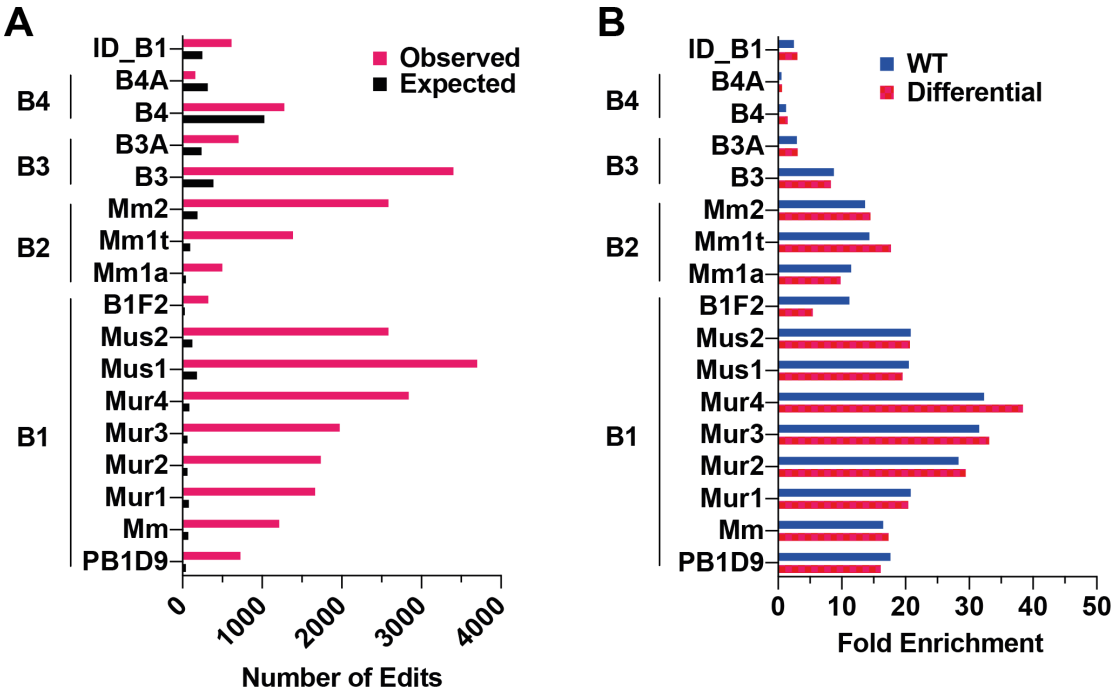

Figure S6. Analysis of RNA editing in SINEs. Related to Figure 7.

A. Sub-families of SINEs were analysed as in Figure 6D, but are plotted to include those where observed or expected values exceeded 250.

B. Fold enrichments of editing events were calculated relative to expected numbers of edits for SINE sub-families using editing events detected in WT samples and differentially edited sites.

Table S1. Differentially expressed REs.

REs differentially expressed in *Adar1* $^{mZ\alpha/mZ\alpha}$ lungs are shown with their log2 fold change and adjusted p-value. The RE class, family and chromosomal location are indicated. REs were sorted by adjusted p-value. The cut-offs used were: log2 fold-change >1 or <-1, and adjusted p-value <0.01.

Class|Family|Chr|Start|Stop	log2 fold change	padj
Satellite|GSAT_MM|JH584304.1|60177|60876	3.3	0
LTR/ERVL-MaLR|MTD|JH584304.1|61136|61478	3.3	6.80E-259
LTR/ERVL-MaLR|MTD|JH584304.1|25102|25465	3.0	4.93E-157
LTR/ERVL-MaLR|MTD-int|5|120880478|120881813	3.3	1.00E-100
LTR/ERVK|ETnERV2-int|18|60283765|60287191	2.1	4.51E-93
LINE/L1|L1MdA_VII|18|60302236|60308420	1.9	4.12E-82
LTR/ERVL-MaLR|MTD-int|5|120900459|120901797	2.3	9.73E-59
LINE/L1|L1M5|5|120744115|120744500	2.8	5.45E-56
LINE/L1|Lx8b|18|60290416|60292037	1.9	1.30E-51
LTR/ERVK|ERVB4_1-I_MM~RLTR50B|18|60288796|60289913	2.1	1.67E-46
LTR/ERVK|IAPEY3_LTR~IAPEy-int|1|173572498|173580638	1.1	6.52E-44
LINE/L1|Lx7|3|151733082|151735087	2.7	1.69E-42
SINE/B4|B4A|5|120879672|120879973	3.9	2.34E-38
SINE/B4|B4A|5|120743868|120744091	2.5	6.13E-38
LINE/L1|L1MdTf_III|7|104475378|104477900	1.6	1.40E-37
SINE/B2|B3|JH584304.1|61870|61954	2.8	7.81E-37
SINE/B2|B2_Mm2|5|120744880|120745045	2.8	5.86E-36
LTR/ERVK|ERVB2_1-I_MM~RLTR13D2|1|173566173|173572495	1.0	3.47E-35
LTR/ERVK|RLTR33|12|103438085|103438897	1.7	9.56E-35
LINE/L1|L1MdN_I|18|60219113|60220489	1.7	1.00E-33
LTR/ERV1|RLTR6-int|12|103440882|103441504	1.9	2.23E-32
SINE/B4|RSINE1|5|120744507|120744635	3.5	7.38E-32
LINE/L1|Lx8|5|114904191|114904607	1.9	1.11E-26
SINE/B2|B3|5|120744692|120744879	2.9	3.76E-26
LINE/L1|L1MdA_I|7|104502396|104504479	1.5	4.46E-25
LTR/ERVK|RMER12B|18|60308716|60309841	1.7	4.59E-25
LTR/ERVK|ETnERV2-int|18|60287718|60288163	2.1	5.34E-25
SINE/B4|B4A|5|120899645|120899943	2.3	9.68E-25
LTR/ERV1|RLTR1A2_MM|18|60287192|60287717	2.2	3.30E-24
LINE/L1|L1MdF_I|7|104489329|104493378	1.6	5.47E-24
LTR/ERVL-MaLR|MTD~MTD-int|5|120867256|120868952	2.7	2.72E-23
LINE/L1|Lx8b|18|60292356|60292908	2.1	7.39E-23
LINE/L1|Lx3_Mus|1|173476327|173479976	1.8	3.80E-22
LINE/L1|L1MdF_III|7|104412877|104415655	1.0	8.14E-22
LINE/L1|Lx7|3|151735621|151736718	2.5	1.26E-21
LINE/L1|L1MdF_IV|18|60258255|60262863	1.8	4.41E-21
LTR/ERVK|RLTR10-int|7|104417226|104418855	1.0	5.22E-21
LTR/ERVL-MaLR|MTA_Mm|5|114907656|114908049	2.1	5.94E-21
LTR/ERVK|RMER19B|11|119395887|119396564	1.3	7.35E-21
LTR/ERVK|MurERV4-int|11|119398983|119400690	1.1	4.62E-20
LTR/ERVK|RLTR13B1|5|120894364|120895346	2.3	1.73E-19
SINE/B4|B4A|5|120732706|120732910	2.6	2.17E-19
SINE/ID|ID2|5|114901484|114901562	1.8	7.16E-19
SINE/B2|B2_Mm2|5|114910369|114910572	2.2	1.60E-18
LINE/L1|L1MdF_III|7|104456010|104461764	1.4	6.23E-18
LINE/L1|L1MdF_IV|8|62028789|62032657	1.4	6.98E-18
LTR/ERVK|RLTR11A2|15|77730371|77730874	2.9	8.25E-18
LTR/ERVK|RLTR10~RLTR10-int|7|104415825|104417145	1.1	1.24E-17
LINE/L1|L1MdA_III|18|60218363|60219112	1.5	3.04E-17
LINE/L1|Lx8|11|48893355|48894122	2.5	4.36E-17
LINE/L1|Lx5|18|60255846|60257256	1.8	5.14E-17
LINE/L1|Lx9|11|48988698|48990056	1.6	8.90E-17
LTR/ERV1|LTR72_RN|18|60217070|60217447	1.6	1.33E-16

LINE/L1|L1MC5|3|151741122|151741823	2.9	1.94E-16
LTR/ERVK|ERVB2_1A-I_MM~RLTR13D5|18|60282851|60283792	1.9	3.57E-16
LTR/ERVK|RLTR17D_Mm|18|60255056|60255845	2.1	4.71E-16
LINE/L1|L1MdF_I|1|85299575|85304519	2.8	5.46E-16
SINE/B2|B3|18|60247949|60248146	1.9	1.13E-15
LINE/L1|L1MEc|16|97458642|97459049	3.0	2.18E-15
LTR/ERVL-MaLR|ORR1C2|5|120748110|120748423	2.8	5.32E-15
LINE/L1|L1MdTf_III|6|57628358|57634538	1.1	6.33E-15
LINE/L1|Lx6|2|173195005|173200024	1.8	7.37E-15
LTR/ERVL-MaLR|ORR1A2|18|60292038|60292355	2.4	7.76E-15
LINE/L1|L1MdV_III|5|120882900|120884828	4.1	9.71E-15
SINE/B4|B4A|5|120737450|120737698	2.8	1.24E-14
LTR/ERVL-MaLR|MTD|X|112371164|112371262	2.3	1.28E-14
LTR/ERVL-MaLR|MTD|11|72304177|72304543	1.2	1.44E-14
SINE/Alu|B1_Mur2|5|120731990|120732119	3.1	2.38E-14
LTR/ERVL-MaLR|MTD~MTD-int|5|120817871|120818905	1.4	2.75E-14
LINE/L1|L1M5|6|3341749|3341957	1.1	3.15E-14
LTR/ERVL-MaLR|MTEb|19|34585573|34585953	2.0	4.45E-14
LINE/L1|L1MdV_III|7|104493403|104495643	1.5	4.59E-14
SINE/B2|B3|5|120745046|120745085	2.7	1.17E-13
LINE/L1|L1MdN_I|7|104477902|104478732	1.3	1.60E-13
LINE/L1|Lx8|18|60212692|60213382	1.6	1.71E-13
LINE/L1|L1MdTf_III|18|60236091|60238578	1.6	2.06E-13
LTR/ERVK|ERVB5_1-I_MM|11|83007973|83009733	1.7	3.34E-13
LINE/L1|L1_Mur3|8|61931617|61933065	1.3	4.13E-13
LINE/L1|L1MdF_IV|18|60231803|60232768	1.7	5.15E-13
LTR/ERV1|MLTR14|7|104421879|104422356	1.2	5.39E-13
LTR/ERVL-MaLR|MTC|16|97454326|97454700	2.7	6.93E-13
LTR/ERVL-MaLR|MTB_Mm-int|17|78862042|78863246	1.0	7.35E-13
DNA/hAT-Charlie|MER58A|5|120899366|120899528	2.4	1.55E-12
LTR/ERVL|RMER15-int|18|60388388|60389084	1.4	2.49E-12
LINE/L1|L1MdF_III|1|52127797|52128672	1.2	3.84E-12
LTR/ERVL-MaLR|ORR1E|11|72305310|72305625	1.2	3.84E-12
LTR/ERVK|RMER19C|5|120739285|120739711	3.8	3.85E-12
LINE/L1|L1MdV_III|7|104450903|104454061	1.4	4.92E-12
SINE/Alu|PB1D9|19|34586260|34586378	2.0	5.01E-12
LINE/L1|Lx5|8|61953216|61953896	1.6	5.84E-12
LINE/L1|L1MdA_III|7|104497785|104499051	1.6	6.75E-12
LTR/ERVK|RLTR10F|5|120745593|120745641	2.3	9.12E-12
LTR/ERVL|MT2C_Mm|12|103431337|103431828	3.1	1.01E-11
LINE/L1|L1MdF_IV|18|60263356|60264933	2.1	1.21E-11
SINE/Alu|B1_Mus1|5|114898644|114898789	2.0	1.28E-11
LINE/L1|Lx8|5|114904021|114904128	2.4	1.34E-11
LTR/ERVL-MaLR|ORR1C1~ORR1C1-int|8|62019273|62020492	1.8	1.82E-11
LTR/ERVL-MaLR|MTD|16|97459784|97460166	2.5	2.57E-11
LTR/ERV1|MER65-int|18|60215493|60215799	1.7	2.61E-11
LINE/L1|Lx7|8|61930625|61931615	1.5	2.77E-11
LINE/L1|L1MdV_I|7|104473898|104475381	1.4	3.00E-11
LTR/ERVL-MaLR|ORR1A4~ORR1A4-int|8|61959410|61960410	1.7	3.12E-11
LTR/ERVL-MaLR|ORR1E|16|97455751|97456075	3.0	3.63E-11
LTR/ERVL-MaLR|MTC|3|151744695|151745110	2.6	4.72E-11
DNA/TcMar-Tigger|Tigger13a|19|28642966|28643654	9.3	5.06E-11
LINE/L1|L1MEc|16|97460167|97460362	3.3	7.07E-11
LTR/ERVK|RMER19B|17|78878705|78879529	1.2	8.11E-11
SINE/Alu|B1F2|5|114899111|114899246	2.1	8.42E-11
LINE/L1|Lx8|8|61978737|61979085	1.7	8.42E-11
LTR/ERVK|RLTR17D_Mm|18|60228369|60229159	1.5	1.01E-10
LINE/CR1|X6A_LINE|6|127449631|127450147	1.7	1.08E-10
SINE/B4|B4|11|119418705|119418955	1.3	1.62E-10
LTR/ERVL|RMER10B|12|103434622|103435041	1.8	2.64E-10
LINE/L1|Lx4A|7|104462257|104463184	1.7	2.88E-10
SINE/Alu|B1_Mur1|11|119424502|119424651	1.2	2.88E-10
LTR/ERVL-MaLR|ORR1A4-int|8|61961707|61963155	1.3	3.22E-10

LTR/ERV1|RLTR1B|16|97457671|97458166	2.2	3.52E-10
SINE/B2|B3A|11|119404723|119404878	1.3	3.77E-10
LTR/ERVL-MaLR|MTC|18|60381338|60381622	1.7	3.77E-10
LINE/L1|L1MdV_I|5|105283637|105285975	1.6	3.97E-10
LTR/ERVK|RLTR25B|19|34650691|34651330	1.4	4.78E-10
SINE/B2|B3|5|114899419|114899545	2.0	6.53E-10
LTR/ERVL|RMER15|19|28639198|28639693	8.9	6.63E-10
LINE/L1|L1_Mur3|16|97548067|97549012	1.7	7.03E-10
LINE/L1|L1MEi|19|28631069|28632121	8.8	8.12E-10
LTR/ERVK|RLTR25A|8|61972997|61973607	1.4	8.16E-10
LINE/L1|L1MdA_VII|18|60288431|60288795	1.8	1.45E-09
LINE/L1|L1Lx_III|3|151742481|151742961	2.4	1.67E-09
LTR/ERVK|MurERV4-int|11|119401805|119402501	1.3	1.86E-09
SINE/B2|B3|X|112370657|112370771	2.0	2.38E-09
LTR/ERVK|MurERV4-int|11|119400881|119401263	1.3	2.38E-09
LINE/L1|Lx9|JH584304.1|46386|46861	1.1	2.46E-09
LTR/ERVK|RMER17B|5|120869622|120870528	2.9	2.74E-09
LTR/ERVL-MaLR|MTB_Mm|15|77733815|77734092	3.4	3.12E-09
LTR/ERVK|ERVB2_1-I_MM|1|173580639|173582295	1.1	3.35E-09
LTR/ERVL-MaLR|ORR1B2|5|114908516|114908882	1.5	4.45E-09
LTR/ERVK|MYSERV-int|6|57638599|57641256	1.0	6.35E-09
SINE/B4|B4|11|119446380|119446625	1.0	7.11E-09
LTR/ERVK|ERVB4_1-I_MM|18|60288165|60288430	1.8	9.39E-09
LTR/ERVL-MaLR|MLT1A|18|60223904|60224219	1.5	1.15E-08
SINE/B2|B2_Mm2|19|34584659|34584843	2.2	1.27E-08
LTR/ERVL-MaLR|MTE2b|8|61970047|61970414	1.6	1.28E-08
LTR/ERVK|ERVB5_1-I_MM|11|83010068|83011537	1.5	1.51E-08
LTR/ERV1|MLTR14|7|104480250|104480718	1.3	1.59E-08
LTR/ERVL-MaLR|MTE2b|1|52136423|52136770	1.1	1.59E-08
SINE/B4|B4A|5|120741648|120741943	2.5	1.60E-08
LINE/L1|Lx8|19|28632845|28633192	8.4	1.81E-08
LINE/L1|Lx2A1|18|60277986|60280175	2.3	1.82E-08
LINE/L1|Lx3_Mus|18|60295395|60298143	1.8	1.91E-08
LINE/L1|L1MEc|16|97459476|97459783	2.7	2.30E-08
LTR/ERVL-MaLR|MTD|5|120900388|120900472	3.2	2.76E-08
LINE/L1|L1M4|16|97553934|97554356	2.3	2.81E-08
LTR/ERVK|IAPLTR2_Mm|3|151740656|151741121	2.1	3.42E-08
LINE/L1|L1MdV_III|7|104488452|104489331	1.6	3.71E-08
LTR/ERVK|MERVK26-int~RLTR26_Mus|7|104448877|104450693	1.2	4.13E-08
SINE/Alu|B1_Mus2|18|60251725|60251812	2.6	4.69E-08
LTR/ERVL-MaLR|ORR1B1|11|119404156|119404499	1.0	6.92E-08
SINE/B2|B2_Mm1t|5|114909495|114909661	2.2	7.44E-08
SINE/B4|RSINE1|11|119425189|119425383	1.2	7.93E-08
SINE/B2|B3A|18|60380840|60381056	1.7	8.13E-08
SINE/B4|B4|19|28629227|28629484	8.2	9.75E-08
LTR/ERVK|RLTR42-int|17|36238528|36239128	4.8	1.06E-07
LTR/ERVL-MaLR|MTC|18|60382046|60382401	1.4	1.18E-07
SINE/B4|ID_B1|11|119407311|119407556	1.0	1.18E-07
DNA/hAT-Charlie|Charlie16a|1|52132936|52133086	1.3	1.23E-07
LTR/ERVL-MaLR|MTB|16|97458167|97458530	2.0	1.37E-07
LINE/L1|L1MC5|18|60271813|60272228	2.2	1.40E-07
SINE/B4|RSINE1|5|120877997|120878148	3.8	1.42E-07
LINE/L1|Lx3_Mus|1|173583337|173589127	1.4	1.42E-07
LINE/L1|L1M2|18|60252957|60253392	2.0	1.47E-07
LTR/ERV1|LTRIS4A|5|114905222|114905693	2.1	1.84E-07
LINE/L1|Lx8|8|61926037|61926661	2.5	1.95E-07
SINE/B2|B3|11|119408463|119408535	1.4	2.06E-07
SINE/Alu|PB1D11|5|114900810|114900897	2.0	2.39E-07
LINE/L1|Lx5|1|85293799|85295584	3.7	2.48E-07
LTR/ERVK|RLTR13D3|18|60232779|60233438	1.8	2.54E-07
LTR/ERVL-MaLR|MTD|5|120737214|120737449	3.1	2.65E-07
LTR/ERVL-MaLR|MTEb|16|97450859|97451049	3.4	2.73E-07
SINE/B4|B4A|18|60257733|60257992	1.7	2.89E-07

LTR/ERVK|MLTR25A|8|61960825|61961601	1.7	2.89E-07
LTR/ERVK|RLTR20A2B_MM|1|52124850|52125329	1.2	3.05E-07
SINE/Alu|B1_Mus1|17|35395764|35395900	1.1	3.22E-07
LINE/L1|L1Lx_III|7|104442758|104443886	1.4	3.32E-07
LTR/ERVL|RMER15-int|18|60217650|60217971	1.2	3.36E-07
DNA/hAT-Charlie|MER20|1|52158511|52158655	1.3	3.50E-07
LINE/L1|L1_Mur3|18|60226049|60226282	2.1	3.64E-07
LTR/ERVK|RLTR20C1_MM|5|120734599|120734859	4.1	4.08E-07
LTR/ERVL-MaLR|MTEb|11|119419503|119419749	1.3	4.17E-07
DNA/hAT-Charlie|MER33|19|28641324|28641627	7.9	4.22E-07
LTR/ERVL-MaLR|MLT1A|18|60250995|60251268	1.7	4.23E-07
LINE/L1|L1MdF_I|11|119397535|119397973	1.3	4.23E-07
SINE/Alu|B1_Mur4|5|114900337|114900479	1.6	4.29E-07
LINE/L1|L1_Mur2|5|105281882|105283598	1.7	4.42E-07
Other|RMER1A|8|61979640|61980291	1.5	4.58E-07
LTR/ERVK|ETnERV2-int|8|62007507|62009017	1.6	4.83E-07
LINE/L1|L1MC5|3|151743348|151743525	2.7	5.34E-07
LTR/ERVL-MaLR|MTD|12|26472066|26472478	2.0	5.39E-07
LINE/L1|L1MB1|18|60220588|60220785	1.4	5.59E-07
SINE/B4|ID_B1|2|173207281|173207474	1.9	5.93E-07
SINE/B4|ID_B1|11|119425805|119425924	1.3	6.35E-07
LTR/ERVL-MaLR|ORR1A2|5|120740579|120740914	3.0	6.88E-07
LINE/L1|Lx4A|7|104437169|104438548	1.4	7.31E-07
LTR/ERVK|ERVB5_1-I_MM|11|83006799|83007974	1.4	9.02E-07
LINE/L1|L1M5|1|78402205|78403427	1.1	1.01E-06
SINE/B2|B2_Mm2|5|114910612|114910685	2.4	1.06E-06
SINE/B4|B4A|1|52129374|52129536	1.4	1.22E-06
SINE/B2|B2_Mm2|19|28642281|28642465	7.7	1.38E-06
SINE/B2|B3|19|28633498|28633654	7.7	1.38E-06
LINE/L1|Lx2B2|11|49062198|49062461	1.2	1.47E-06
LTR/ERV1|MER34A|6|57582287|57582506	1.1	1.49E-06
LINE/L1|L1MdF_I|GL456221.1|2915|7856	2.8	1.54E-06
LTR/ERVL|MLT2D|11|48885340|48885618	2.4	1.54E-06
LTR/ERVK|MMERVK9E_I-int|8|62004675|62005632	1.5	1.72E-06
LINE/L1|Lx8|18|60239540|60240228	1.8	1.84E-06
LTR/ERVK|BGLII|7|104482055|104482477	1.4	2.15E-06
LTR/ERVK|RMER6C|2|173214417|173215067	2.6	2.19E-06
LTR/ERVL-MaLR|MTEa-int|1|85289885|85291027	7.6	2.30E-06
LTR/ERVL-MaLR|ORR1C2|2|131068596|131068990	1.1	2.40E-06
LTR/ERVL-MaLR|ORR1F|18|60253720|60254029	2.1	2.42E-06
LTR/ERVK|RMER12|5|120762281|120763522	3.3	2.49E-06
SINE/B4|RSINE1|4|99841078|99841236	7.6	2.59E-06
LINE/L1|Lx4A|7|104504433|104505979	1.4	2.59E-06
LTR/ERVL-MaLR|MTD-int|5|120819453|120820125	1.2	2.78E-06
LINE/L1|L1MC|11|58190640|58190990	1.4	3.05E-06
LINE/L1|L1MdFanc_I|8|62027358|62028774	1.4	3.18E-06
LINE/L1|L1MdF_V|6|57656263|57657234	1.6	3.19E-06
SINE/B4|B4A|11|119428315|119428565	1.8	3.55E-06
LTR/ERVK|RLTR31B2|11|48886943|48887241	2.0	3.61E-06
LINE/L1|L1MEg|14|22926181|22927055	1.2	3.61E-06
LTR/ERVL-MaLR|MLT1A|18|60248622|60248960	1.5	3.84E-06
LTR/ERVL-MaLR|MLT1E1A|8|61928913|61929235	1.9	4.17E-06
LINE/L1|Lx8|18|60383318|60384031	1.1	4.25E-06
LTR/ERVL-MaLR|MTA_Mm~MTA_Mm-int|19|56257034|56258929	1.3	4.57E-06
LINE/L1|L1MCc|1|173466324|173466705	2.3	4.62E-06
LINE/L1|L1Lx_IV|11|82998919|83000309	1.6	4.81E-06
SINE/B4|B4A|5|120741975|120742193	2.7	4.96E-06
SINE/B4|B4A|19|28635419|28635576	7.6	4.96E-06
SINE/B4|ID_B1|11|119403020|119403132	1.2	5.58E-06
LINE/L1|L1M5|18|60226313|60226492	2.0	5.89E-06
LTR/ERVL-MaLR|ORR1A3|11|119407950|119408239	1.1	6.40E-06
LINE/L1|L1MC|11|58189736|58190050	1.3	7.01E-06
SINE/B2|B3A|8|61987073|61987211	1.7	7.39E-06

LTR/ERVK|RMER20B|3|151742296|151742480	2.7	8.09E-06
SINE/B4|RSINE1|16|97453740|97453952	2.7	8.54E-06
LTR/ERVL-MaLR|ORR1G|18|60226675|60226792	2.8	8.94E-06
LTR/ERV1|LTR72_RN|18|60387696|60387959	1.2	9.12E-06
SINE/B4|ID_B1|12|26447776|26447975	4.2	1.01E-05
LTR/ERVL-MaLR|ORR1B1-int|7|104412596|104412775	1.4	1.03E-05
SINE/Alu|PB1D10|5|114903889|114904001	2.0	1.07E-05
DNA/hAT-Charlie|MER20|5|120732243|120732442	2.4	1.21E-05
LTR/ERVK|MLTR18D_MM|19|34642526|34643041	1.5	1.27E-05
LTR/ERVL-MaLR|ORR1F|16|97539474|97539795	2.5	1.37E-05
LTR/ERVL-MaLR|MTE2a|18|60222383|60222695	1.5	1.38E-05
LTR/ERVK|MLTR25A|8|61972378|61972814	1.4	1.49E-05
LTR/ERVL-MaLR|MTD~MTD-int|11|119438208|119439017	1.3	1.60E-05
LINE/L1|Lx8b|7|104422425|104422813	1.0	1.60E-05
SINE/Alu|B1_Mur2|11|58189251|58189397	1.2	1.60E-05
SINE/B2|B2_Mm2|5|114900909|114901081	1.9	1.64E-05
LTR/ERVK|RMER6D|8|61937912|61938757	1.4	1.74E-05
LINE/L1|L1MdF_IV|14|59239026|59244038	1.0	1.75E-05
LTR/ERVL-MaLR|MTB_Mm|15|77406091|77406368	4.2	1.89E-05
SINE/Alu|B1_Mus1|18|60224405|60224548	2.0	1.89E-05
SINE/Alu|B1_Mur3|11|119403373|119403524	1.5	1.89E-05
LTR/ERVK|RMER17D|18|60376370|60377162	1.3	2.06E-05
LINE/L1|L1MdGf_II|8|61952074|61952803	1.6	2.07E-05
SINE/B2|B3A|5|120736482|120736718	2.9	2.09E-05
LTR/ERVK|RMER20B|3|151742962|151743316	1.9	2.12E-05
SINE/B4|RSINE1|4|99840780|99840864	7.3	2.22E-05
LTR/ERVK|RLTR10|7|104415656|104415786	1.3	2.23E-05
LTR/ERVL-MaLR|MTD|6|121255828|121256203	1.2	2.24E-05
LTR/ERVK|RMER6C|8|62032655|62033307	2.1	2.33E-05
LINE/L1|L1MdFanc_II|11|48895925|48896912	2.5	2.39E-05
LTR/ERVL-MaLR|MTD|1|52138546|52138957	1.1	2.40E-05
LINE/L1|Lx2B2|11|48990324|48990587	1.8	2.56E-05
SINE/B4|B4A|11|72310037|72310328	1.2	2.56E-05
LINE/L1|Lx8b|18|60275235|60275895	3.0	2.59E-05
LTR/ERVK|MMERVK9E_I-int|8|62005696|62006980	1.4	2.65E-05
LINE/L1|Lx8b|6|57648031|57648834	1.0	2.83E-05
SINE/B2|B3A|5|120906530|120906727	2.1	2.97E-05
LINE/L1|L1M2|6|121257693|121258500	1.2	3.22E-05
LINE/L1|L1MdF_V|7|105888905|105891419	1.0	3.33E-05
SINE/B4|B4A|18|60222757|60223022	1.4	3.54E-05
LINE/L1|L1MdMus_I|7|105905000|105906394	1.1	3.88E-05
SINE/B2|B3|18|60223226|60223431	1.4	3.95E-05
LINE/L1|L1MEc|16|97540878|97541130	2.8	3.98E-05
LTR/ERVL-MaLR|ORR1B1|10|128274867|128275232	1.1	3.98E-05
SINE/B2|B2_Mm2|5|120736758|120736943	3.2	4.16E-05
LTR/ERVK|RMER6A|8|61944108|61944875	2.1	4.30E-05
SINE/B2|B2_Mm2|17|78880852|78881043	1.4	4.30E-05
LINE/L1|L1M5|8|61946379|61947158	1.8	4.69E-05
SINE/Alu|B1_Mus1|5|114909326|114909471	1.9	4.70E-05
LINE/L1|Lx5|11|48881306|48882584	2.4	4.97E-05
LINE/L1|Lx8|11|78973853|78974577	1.0	5.04E-05
SINE/B2|B2_Mm2|19|28632419|28632602	7.2	5.25E-05
LTR/ERVK|ERVB4_1C-LTR_Mm|1|52125995|52126510	1.1	5.62E-05
LTR/ERVL-MaLR|MTC|14|59357742|59357949	1.4	5.66E-05
LTR/ERVK|ERVB5_1-I_MM~ERVB5_2-LTR_MM|11|83005040|83006189	1.7	6.18E-05
SINE/B4|RSINE1|18|60213658|60213808	1.6	6.18E-05
LINE/L1|L1MdF_II|6|57667427|57673682	1.1	6.18E-05
LTR/ERVK|RLTR20A3_MM|7|104463189|104463682	1.4	6.53E-05
SINE/Alu|PB1D7|5|120876099|120876194	4.1	6.65E-05
LTR/ERVL-MaLR|MTD|19|34649682|34650059	1.8	6.96E-05
SINE/Alu|B1_Mus2|11|119397366|119397508	1.5	7.02E-05
LTR/ERVL|MT2B1|18|60266284|60266703	2.0	7.08E-05
LTR/ERVL|MT2B2|16|23610543|23610701	1.8	7.08E-05

LINE/L1|L1M5|8|62026273|62026678	1.9	7.22E-05
SINE/B2|B3|11|119431991|119432188	1.5	8.27E-05
LINE/L1|L1MA9|18|60389514|60389752	1.2	8.52E-05
LTR/ERVK|RMER16B2|19|34643495|34643896	1.6	9.10E-05
SINE/B2|B3|11|48885122|48885339	2.9	9.26E-05
LTR/ERVK|RLTR31D_MM|8|61934369|61934756	1.5	9.26E-05
SINE/B4|B4A|1|52121302|52121516	1.5	9.44E-05
LINE/L1|Lx6|2|173200965|173202050	2.1	9.82E-05
LINE/L1|L1MC3|5|100554042|100554239	1.8	0.000109224
LTR/ERVK|ERVB4_1-I_MM~RLTR43C|8|62002691|62003827	1.4	0.000109224
LINE/L1|L1_Rod|6|57584670|57585726	1.1	0.000110408
LTR/ERVK|RLTR33|7|104482478|104483095	1.1	0.000112452
LINE/L1|Lx2A1|18|60275890|60277983	1.7	0.000114821
LTR/ERVL-MaLR|MTC|18|60235502|60235795	1.8	0.000116123
LINE/L1|Lx8|18|60380013|60380364	1.5	0.000116123
LTR/ERVL-MaLR|ORR1F|5|120760326|120760690	2.6	0.00012678
LTR/ERV1|MER65-int|18|60386130|60386423	1.1	0.000133868
LTR/ERVL-MaLR|ORR1A2|1|173467096|173467424	1.9	0.00013703
LINE/L1|Lx8|8|94438097|94440818	1.0	0.000152871
SINE/B2|B3|11|119448108|119448296	1.1	0.000154092
SINE/Alu|PB1|11|119422838|119422954	1.2	0.000158146
LINE/L1|L1ME3A|1|85672489|85672941	1.0	0.000158146
SINE/B2|B2_Mm1t|11|78980069|78980247	1.7	0.000159374
LINE/L1|L1MdFanc_I|8|62026867|62027358	1.8	0.000168661
LTR/ERVL-MaLR|ORR1D1|8|61993767|61994083	1.9	0.000168999
LINE/L1|L1MdF_III|5|109141850|109144085	1.7	0.00017257
LTR/ERVK|RLTR50B|18|60281383|60281838	1.7	0.000172929
LINE/L1|L1MB3|16|97449241|97449562	2.5	0.000177
SINE/Alu|B1_Mur3|16|35844933|35845040	1.2	0.000177668
LTR/ERVK|RLTR17|1|173482685|173483219	2.2	0.000179126
SINE/B2|B3|GL456211.1|227084|227304	3.2	0.000182121
LINE/L1|Lx8|8|61988622|61989015	1.6	0.000186362
LTR/ERVK|RMER17A2|11|48885977|48886924	1.6	0.000186858
LTR/ERVL-MaLR|ORR1D1|8|62016352|62016678	1.9	0.000207871
DNA/TcMar-Tigger|Tigger17a|1|52148302|52148747	1.1	0.000209188
SINE/B4|RSINE1|11|119421171|119421274	1.8	0.000217129
SINE/B4|B4A|5|120866302|120866579	3.2	0.000219053
SINE/B2|B2_Mm1t|11|58190313|58190486	1.4	0.000220304
SINE/B2|B3|14|59352375|59352576	1.4	0.000223123
SINE/Alu|B1_Mus1|18|60249131|60249275	1.6	0.00023365
SINE/B4|ID_B1|1|78411074|78411271	1.5	0.00023459
LTR/ERVK|ERVB4_1-I_MM|18|60282151|60282841	1.8	0.000240016
LINE/L1|Lx7|11|49092819|49093419	1.2	0.000244381
LINE/L1|L1MA9|6|57597772|57598304	1.1	0.000249114
SINE/Alu|B1_Mus1|12|103436139|103436281	1.9	0.00027349
LINE/L1|L1MdA_III|16|36223021|36229214	1.2	0.000274576
SINE/B4|RSINE1|5|120872117|120872273	3.3	0.000287785
LTR/ERVL-MaLR|MTD|11|72309643|72309975	1.1	0.000289508
SINE/B4|B4A|1|173484993|173485286	2.2	0.000290371
SINE/B4|B4A|18|60231038|60231308	1.5	0.000327918
LTR/ERVL-MaLR|MTA_Mm|16|97552450|97552832	1.9	0.000331455
LINE/L1|L1MdV_I|11|119469230|119469675	1.0	0.000339371
SINE/B2|B3A|8|61937106|61937279	1.7	0.000348467
SINE/B2|B3A|17|6453751|6453921	2.1	0.000353282
LTR/ERVL-MaLR|ORR1A2|7|104497343|104497650	1.6	0.00035773
LTR/ERVL-MaLR|ORR1D2-int|7|105893142|105893563	1.0	0.00035773
LINE/L1|Lx8|8|61959169|61959373	1.9	0.000360775
LINE/L1|Lx8|19|12528103|12528695	1.8	0.000365486
LINE/L1|L1MdF_III|7|104454974|104455697	1.4	0.000367396
LINE/L1|L1MdA_IV|11|118381899|118388191	1.3	0.000368207
SINE/Alu|PB1|16|35845564|35845645	1.0	0.000374836
LINE/L1|L1MdA_III|18|60406432|60412549	1.2	0.00038205
LTR/ERVL|RMER10B|16|23611518|23611704	1.8	0.00040784

LINE/L1|Lx7|1|173470250|173470764	1.9	0.000408506
LTR/ERVK|RLTR25A|8|61960411|61960742	2.2	0.000410879
LINE/L1|Lx6|7|104440983|104441613	1.3	0.000418042
SINE/Alu|PB1D10|11|119403173|119403281	1.2	0.000428833
LTR/ERVL-MaLR|ORR1A2|5|120893806|120893895	3.5	0.000439001
LTR/ERVL-MaLR|MLT1A0|3|151744445|151744691	2.5	0.000451551
LTR/ERV1|RLTR23|5|120818906|120819376	1.1	0.000453883
LINE/L1|L1MC5|3|151740389|151740655	2.6	0.000462351
LINE/L1|Lx2B|8|61987536|61987650	2.2	0.000462351
SINE/Alu|B1_Mur3|11|72309443|72309576	1.8	0.000466519
SINE/B2|B3A|5|120886654|120886852	2.8	0.000474244
LTR/ERVL-MaLR|ORR1B2-int|18|60308447|60308715	1.8	0.000476449
LINE/L1|L1Lx_IV|11|83024253|83025643	1.3	0.000478685
SINE/Alu|B1_Mur4|18|60388241|60388387	1.5	0.000504818
LINE/L1|L1MEg|14|22924975|22925754	1.1	0.000521911
LINE/L1|L1MC3|19|12525661|12526010	2.0	0.000523155
SINE/B2|B3|11|119396967|119397132	1.2	0.000532394
LINE/L1|L1MdV_I|6|57655972|57656262	1.8	0.00058615
LTR/ERV1|MER65-int|18|60242375|60242677	2.0	0.000593172
LINE/L1|L1Lx_IV|7|104447255|104447947	1.2	0.000595394
LTR/ERVL|RMER15-int|18|60388050|60388240	1.2	0.000595471
SINE/Alu|B1_Mus1|11|119422309|119422456	1.3	0.000597017
LINE/L1|Lx8|14|59362138|59362787	1.3	0.000608974
LINE/L1|L1MEc|16|97542889|97543268	2.3	0.000613872
LINE/L1|L1Lx_I|8|61950817|61951123	1.7	0.000627706
LINE/L1|Lx3B|18|60271246|60271457	2.0	0.000635352
LTR/ERVK|RLTR33|7|104481788|104482054	1.2	0.000639421
LINE/L1|L1MdA_IV|15|75013194|75019358	1.0	0.000654485
LTR/ERVK|MMERVK10D3_I-int|19|12537134|12538136	1.6	0.00066349
SINE/B4|RSINE1|18|60384304|60384453	1.2	0.000669838
LINE/L1|L1MdA_II|Y|90726495|90727209	6.2	0.000676413
LTR/ERVK|RMER17C2|11|119394660|119395025	1.1	0.000679554
LINE/L1|L1ME2|19|34584395|34584639	1.8	0.000701496
LTR/ERVL|MT2B2|5|114912527|114913101	1.5	0.000762304
LTR/ERVL-MaLR|ORR1C2|11|118395751|118396103	1.6	0.000762944
LTR/ERV1|MMVL30-int|18|60249553|60250002	1.4	0.000823898
SINE/B4|B4|1|173475932|173476222	1.8	0.000849572
SINE/B4|B4A|1|52133585|52133834	1.1	0.000870689
LINE/L1|L1_Mur2|7|104496617|104497342	1.3	0.00094743
SINE/B2|B3A|1|85660064|85660261	1.1	0.000971813
LTR/ERVK|RMER19B|1|85214688|85215577	3.1	0.000987718
SINE/B2|B3A|11|58190051|58190291	1.6	0.001005606
LINE/L2|L2|4|128922527|128922668	2.6	0.001051836
LINE/L1|Lx8b|18|60375408|60375552	2.8	0.001063904
SINE/Alu|B1_Mur1|11|72310329|72310474	1.5	0.00107883
LTR/ERV1|MER34|8|61991169|61991412	1.3	0.001089669
SINE/Alu|B1_Mus1|18|60251484|60251628	2.4	0.00110542
LINE/L1|L1_Rod|16|97549085|97549369	1.8	0.001150467
SINE/B4|B4A|5|120742594|120742675	2.3	0.001173077
SINE/B4|ID_B1|5|120736246|120736457	2.4	0.001203452
LINE/L1|L1MdGf_I|4|96209256|96210247	5.5	0.001205117
LINE/L1|Lx7|11|48898552|48898950	3.0	0.001264124
SINE/B4|B4A|8|61938958|61939194	1.9	0.001273237
SINE/B4|B4A|12|26455259|26455616	3.1	0.001297065
SINE/B4|RSINE1|3|151741825|151741992	2.3	0.001354579
LINE/L2|L2c|17|78881711|78882045	1.3	0.001408036
SINE/Alu|B1_Mur3|11|119427174|119427277	1.3	0.001415298
LINE/L1|L1M5|6|57664127|57664870	1.4	0.001441351
LTR/ERVL|RMER10A|11|58191702|58192067	1.4	0.001493181
SINE/B2|B3|1|78405712|78405917	1.4	0.001633648
LINE/L1|L1M2|18|60245064|60245319	1.7	0.001694221
SINE/Alu|PB1D10|11|119474405|119474499	1.6	0.001812519
LINE/L1|L1M1|1|78410131|78410363	1.3	0.001823318

LTR/ERVL|LTR53-int|8|61923911|61924391	2.0	0.001837723
DNA/TcMar-Tc1|EutTc1-N2|7|104499725|104499945	1.4	0.001884216
SINE/B2|B3A|8|61970949|61971157	1.6	0.001896582
LINE/L1|L1MC4|6|121243607|121243843	2.9	0.001905609
LTR/ERVL|RMER15-int|18|60243994|60244664	1.5	0.001914539
LINE/L1|L1MdF_I|GL456221.1|185129|190073	2.1	0.00193405
LINE/L1|L1MdGf_II|7|104461765|104462256	1.8	0.001965446
SINE/B2|B2_Mm1t|5|120742377|120742561	2.4	0.001970116
SINE/B2|B3A|18|60234288|60234503	1.9	0.001990529
Unknown|YREP_Mm|18|60224643|60224761	1.7	0.002034878
LTR/ERV1|RodERV21-int|5|38628522|38629464	2.3	0.002074407
LTR/ERVL-MaLR|ORR1G|18|60227122|60227332	1.4	0.002074407
LTR/ERVK|ERVB5_2-LTR_MM|11|83011538|83011994	1.7	0.002105801
LINE/L1|L1MC5a|5|120729622|120729973	3.3	0.002120947
LINE/L1|L1MdA_VII|14|22550685|22551432	1.3	0.002120947
SINE/B2|B3A|8|61929572|61929765	1.8	0.002135782
SINE/B4|RSINE1|1|52121688|52121837	1.5	0.002244338
SINE/B2|B3|18|60250421|60250516	1.8	0.00227286
SINE/Alu|B1_Mus1|5|120737774|120737916	2.2	0.002313263
LINE/L1|L1MdV_III|1|173472409|173472805	2.1	0.002313263
LINE/L1|L1MdTf_I|11|11287224|11294492	1.4	0.002358409
SINE/B4|B4A|5|120869392|120869621	3.0	0.002427648
LINE/L1|L1MD2|1|78415831|78416284	1.1	0.002580399
DNA/hAT-Charlie|URR1A|8|61989152|61989341	1.8	0.002588266
SINE/B4|B4A|10|128280206|128280475	1.1	0.002608665
SINE/B4|ID_B1|6|121257175|121257271	2.3	0.0026213
SINE/B2|B2_Mm2|11|58205520|58205716	1.8	0.002654082
LINE/L1|L1M3|7|104480884|104481245	1.2	0.002675589
SINE/B2|B2_Mm2|4|128922392|128922528	2.7	0.002693458
LTR/ERVL-MaLR|MLT1A0|16|97552073|97552408	1.8	0.002912433
LINE/L1|L1M3|18|60225894|60226042	2.4	0.002922993
SINE/Alu|B1_Mur4|11|119432213|119432355	1.4	0.002957208
SINE/B4|B4A|11|119454023|119454233	1.1	0.003132828
LTR/ERVK|RLTR25A|1|85292929|85293798	2.8	0.003188085
SINE/B4|RSINE1|5|120734442|120734572	3.4	0.003210838
SINE/B2|B3A|8|62017361|62017545	2.3	0.003228318
SINE/B4|B4|5|120814775|120815080	1.3	0.003330175
SINE/B2|B3|2|122154363|122154562	1.0	0.003385239
SINE/B4|B4A|12|103430589|103430874	2.6	0.003428791
DNA/hAT-Charlie|URR1B|6|57634600|57634757	1.5	0.003486983
LINE/L1|Lx5c|3|151730142|151730853	2.7	0.003555802
LTR/ERVK|MMERVK10D3_I-int~RLTR10D2|4|156157848|156161930	1.2	0.003555802
SINE/B2|B3|11|119403552|119403719	1.1	0.003661118
SINE/B2|B2_Mm2|11|119474900|119475066	1.4	0.003666262
SINE/Alu|B1_Mur1|11|119426938|119427074	1.2	0.003667705
LTR/ERVK|RMER17C2|11|48891203|48891735	2.0	0.003754317
LINE/L1|L1MdA_VI|18|60412548|60416252	1.5	0.003804298
SINE/Alu|PB1|11|119415833|119415919	1.3	0.00384182
LTR/ERVK|RMER4A|1|52145655|52146094	1.1	0.003931657
SINE/B4|ID_B1|1|78408347|78408481	1.3	0.004223362
LTR/ERVK|RLTR53_Mm|3|7605461|7605702	1.2	0.004487373
SINE/B2|B3A|14|59352033|59352172	1.1	0.004525402
LTR/ERVL|LTR33|8|61980345|61980747	1.4	0.004585898
LINE/L1|Lx8|11|48897140|48897506	2.9	0.00469754
SINE/MIR|MIR|11|78984217|78984391	1.2	0.004703329
SINE/Alu|B1_Mur4|1|85678728|85678875	1.1	0.004703329
SINE/B2|B3|1|85699200|85699407	1.1	0.004748338
SINE/B2|B3A|11|119453072|119453230	1.1	0.004748338
LTR/ERV1|LTR72_RN|18|60243439|60243666	1.9	0.004758321
SINE/Alu|B1_Mm|JH584304.1|45633|45776	1.0	0.004811999
SINE/Alu|B1F|19|34589599|34589737	1.8	0.004941696
LTR/ERVK|MurERV4-int~RMER4B|5|38640610|38642621	1.8	0.005052178
SINE/Alu|B1F|17|36016700|36016833	1.0	0.005108486

LTR/ERVK|RLTR11A2|14|74841714|74841956	1.5	0.005149262
LINE/L1|L1M3|5|105287249|105287488	2.1	0.005207743
LINE/L1|L1ME2|19|34608766|34609012	1.6	0.005229814
LTR/ERVL-MaLR|ORR1B1|1|85206513|85206871	2.0	0.00524806
SINE/B2|B3|12|103430943|103431152	2.7	0.005295518
SINE/B2|B3|5|120742194|120742376	2.2	0.005295518
LTR/ERVK|MLTR11B|8|61922797|61923291	2.5	0.005350656
SINE/B4|B4A|3|151732580|151732796	2.2	0.005350656
LTR/ERVK|RMER17A2|11|83025644|83026552	1.4	0.005414877
SINE/Alu|B1_Mur1|5|120741326|120741462	2.2	0.005446161
LINE/L1|Lx9|8|61996144|61997073	1.4	0.005583858
LTR/ERVK|RLTR12BD_Mm|11|119413650|119414012	1.4	0.005603168
LINE/L1|Lx7|5|81690438|81691087	1.2	0.00570399
LINE/L1|Lx5b|16|97541515|97541575	3.7	0.00581336
LTR/ERVL-MaLR|MTC|18|60234785|60235077	1.8	0.005929058
LINE/L1|L1MC4|1|105984514|105984997	1.5	0.006181554
LINE/L1|Lx6|3|151725975|151728003	2.7	0.006490343
LTR/ERV1|MLTR14|11|119393861|119393938	1.2	0.006490343
LINE/L1|L1MdFanc_I|8|61966298|61966923	1.6	0.006798172
Unknown|MurSatRep1|8|61986589|61986618	2.1	0.006944851
LTR/ERVK|RMER6C|1|173466744|173467049	1.9	0.007173117
LTR/ERVL|RMER15|16|97552833|97553254	1.7	0.007459961
SINE/Alu|B1F1|10|128273839|128273957	1.2	0.007468964
LINE/L1|L1MdA_V|1|147487927|147488645	1.1	0.007581135
SINE/Alu|B1_Mur2|11|119422475|119422589	1.1	0.007632876
SINE/B2|B3|1|52161968|52162165	1.3	0.007756351
SINE/B2|B3|14|59244430|59244631	2.6	0.00778006
SINE/B4|RSINE1|16|35862636|35862773	1.1	0.007852115
LTR/ERVL-MaLR|ORR1D1|11|78966330|78966666	1.1	0.007852374
SINE/Alu|PB1D10|1|52157797|52157904	1.1	0.00786182
LTR/ERVL-MaLR|ORR1E|16|97545892|97546219	1.6	0.007932381
LTR/ERVK|RLTR10D2|11|83014754|83015108	1.8	0.00795139
LINE/L1|Lx4B|18|60254283|60254608	1.4	0.008019575
SINE/Alu|PB1|JH584304.1|46147|46243	1.3	0.008096681
SINE/B4|RSINE1|11|119454707|119454839	1.2	0.008275749
SINE/B2|B2_Mm2|11|48892662|48892842	2.2	0.008551993
SINE/B4|ID_B1|10|128280630|128280828	1.1	0.008555514
LTR/ERVL-MaLR|MTC|5|114931510|114931937	4.4	0.008616601
LTR/ERVL|RMER15-int|5|38610880|38612957	1.6	0.008698384
LINE/L1|Lx3_Mus|5|109113342|109113831	2.3	0.008784429
LINE/L1|L1_Mus3|16|35876707|35879416	2.1	0.008815001
LINE/L1|L1MdMus_II|5|109131054|109134304	1.3	0.009424916
SINE/B2|B3A|11|119419727|119419826	1.1	0.009454442
SINE/B2|B3A|16|35855574|35855739	1.0	0.009590665
LTR/ERVL-MaLR|ORR1B1|11|119397240|119397294	1.5	0.009627717
LINE/L1|Lx4B|18|60227587|60227901	1.5	0.009650305
SINE/Alu|B1_Mur2|4|42698174|42698309	-1.2	0.006343316
SINE/Alu|B1_Mus2|14|52188546|52188712	-1.3	0.006282691
SINE/Alu|B1_Mur4|4|42702271|42702324	-1.0	0.00577895
LTR/ERVK|ERVB7_1-LTR_MM~ETnERV-int|7|133528843|133536216	-4.1	0.005738875
LINE/L1|Lx6|5|109930987|109932960	-1.1	0.004709914
LTR/ERVL-MaLR|ORR1A2|4|42198416|42198743	-1.8	0.003795357
LTR/ERVL-MaLR|MTC|4|41860499|41860704	-1.2	0.002380466
LTR/ERVL-MaLR|ORR1D1|5|81438765|81439074	-1.3	0.001738738
LINE/L1|Lx8|5|81442017|81442485	-1.1	0.001387036
SINE/Alu|B1_Mus1|4|42701837|42701939	-1.3	0.001332738
LINE/L1|L1MB4|GL456350.1|213136|214351	-1.3	0.001244243
LINE/L1|Lx3B|1|38194814|38195586	-1.1	0.001203452
SINE/Alu|B1_Mus1|4|42211905|42212047	-3.1	0.000987718
LINE/L1|L1Lx_III|14|22888262|22889657	-1.3	0.00085488
LTR/ERVL-MaLR|MTD|4|42470347|42470605	-1.4	0.000541809
LTR/ERVL-MaLR|MTD|4|42206462|42206627	-1.2	0.000526551

LTR/ERV1|LTRIS2|4|41882251|41882738	-1.9	0.000395352
SINE/B2|B3|4|42006940|42007096	-1.6	0.000368207
LTR/ERVL-MaLR|MTC|4|41859834|41859870	-5.7	0.000364103
LTR/ERVK|RMER17B2|4|42199930|42200852	-1.6	0.000331455
LINE/L1|Lx9|2|106407857|106408375	-1.2	0.000292512
LINE/L1|L1M4b|4|42207136|42207346	-5.0	0.00029125
SINE/Alu|B1_Mus1|14|52189113|52189250	-1.3	0.000225471
LINE/L1|L1MB4|GL456350.1|215333|215759	-1.7	0.000179446
LTR/ERVK|ERVB7_1-LTR_MM~ETnERV-int|3|78552311|78559462	-2.2	0.000126775
LTR/ERVL-MaLR|MTC|4|42209075|42209111	-7.0	8.34E-05
SINE/B4|B4A|4|42205385|42205658	-1.3	7.74E-05
SINE/Alu|B1_Mur4|4|42005473|42005619	-1.2	7.08E-05
SINE/Alu|B1_Mus2|4|42202263|42202409	-1.5	6.34E-05
LTR/ERVL-MaLR|ORR1A3|4|42201549|42201891	-1.4	5.86E-05
DNA/hAT-Tip100|Arthur2|4|41855107|41855330	-1.1	4.99E-05
LTR/ERVK|MMERVK10C-int~RLTR10B2|8|3945964|3951863	-1.1	4.34E-05
LTR/ERVK|RMER17B2|4|41944961|41945909	-1.2	3.08E-05
SINE/B2|B3|4|41846277|41846489	-1.1	2.22E-05
LTR/ERVK|ERVB7_1-LTR_MM~ETnERV-int|3|8383520|8390993	-3.2	1.63E-05
SINE/Alu|B1_Mus2|4|42699410|42699556	-1.1	5.87E-06
SINE/Alu|B1_Mur1|4|42699613|42699730	-1.1	4.11E-06
scRNA|BC1_Mm|JH584293.1|158471|158531	-7.4	2.78E-06
LINE/L2|L2|18|78192885|78194073	-3.5	1.06E-06
LTR/ERVL-MaLR|ORR1B2|4|42210920|42211264	-3.1	9.23E-07
SINE/Alu|B1_Mur3|4|41845780|41845916	-1.2	2.66E-07
LTR/ERVL-MaLR|ORR1E|4|42488823|42489144	-1.6	2.57E-07
SINE/ID|ID4|4|42689431|42689510	-1.2	2.13E-07
SINE/Alu|B1_Mur2|4|42006829|42006920	-1.4	2.08E-07
SINE/Alu|B1_Mur4|4|42693249|42693395	-1.3	1.76E-07
SINE/B4|RSINE1|4|42698000|42698095	-1.3	8.46E-08
LTR/ERVL-MaLR|ORR1A3|4|42698696|42699038	-1.6	4.88E-08
LINE/L1|Lx5|4|42692601|42692763	-1.2	2.87E-08
SINE/B2|B3|4|42677410|42677598	-1.3	1.91E-08
LINE/L1|L1MdTf_I|10|106206469|106213575	-2.0	1.75E-08
LINE/L1|L1MdF_I|4|42699736|42700028	-1.3	1.60E-08
LTR/ERVL-MaLR|ORR1A3|4|42010910|42011252	-1.1	1.44E-08
SINE/B2|B3|4|42694716|42694872	-1.1	1.35E-08
SINE/Alu|B1_Mur2|4|42690321|42690460	-1.1	8.84E-09
LTR/ERVL-MaLR|MTC|4|42208669|42208881	-3.3	5.97E-09
LTR/ERV1|MERV1_I-int~RLTR41|4|41997400|42000692	-1.1	5.26E-09
Unknown|YREP_Mm|4|42698157|42698308	-1.5	3.92E-09
LTR/ERVL-MaLR|MTD|4|42212252|42212563	-3.6	2.84E-09
LTR/ERVL-MaLR|MTD|4|42211419|42211544	-3.1	1.45E-09
LTR/ERVL-MaLR|ORR1E|4|42693396|42693452	-1.4	1.39E-09
LTR/ERVL-MaLR|MTD|4|42703609|42703774	-1.2	1.26E-09
LINE/L1|L1M4b|JH584293.1|158632|158842	-6.4	1.20E-09
SINE/B2|B2_Mm2|4|21873292|21873426	-1.4	9.41E-10
SINE/B2|B2_Mm1t|4|42487831|42488007	-1.5	7.00E-11
SINE/B2|B3|4|42206861|42207067	-2.8	7.19E-12
LTR/ERVL-MaLR|ORR1E|4|42005151|42005472	-1.3	3.84E-12
SINE/B2|B3|4|42692346|42692558	-1.2	1.67E-12
SINE/B2|B2_Mm1t|4|41859871|41860047	-5.8	8.98E-13
LTR/ERV1|LTR72_RN|4|41863323|41863472	-2.5	8.63E-13
SINE/B4|B4A|4|42696105|42696301	-1.5	1.93E-13
LTR/ERVL-MaLR|ORR1D2|4|41866797|41866870	-6.0	3.33E-14
LTR/ERV1|MERV1_I-int~RLTR41|4|42493603|42496895	-1.4	2.28E-14
LTR/ERVL-MaLR|ORR1E|4|42692927|42693248	-1.3	1.71E-14
LTR/ERV1|RLTR1B-int|4|41881485|41882110	-1.4	4.25E-15
LTR/ERVK|IAPEz-int~IAPLTR1_Mm|2|154354263|154359592	-1.0	3.35E-15
LTR/ERVK|ETnERV-int|4|41882740|41882895	-2.4	2.39E-15
LTR/ERVL-MaLR|MTD|4|42703056|42703249	-1.3	1.37E-15
LINE/L1|L1M5|4|42688781|42688992	-1.3	6.88E-16
SINE/Alu|B1_Mur2|4|21872875|21873007	-1.9	9.59E-17

SINE/B2|B3A|4|42688563|42688744	-1.2	6.68E-17
DNA/hAT-Tip100|Arthur2|4|42701104|42701325	-1.3	2.80E-17
SINE/B2|B2_Mm1t|4|42006288|42006464	-1.5	1.95E-17
LINE/L1|Lx9|4|42696517|42697053	-1.3	3.62E-19
SINE/B4|B4A|4|42702532|42702805	-1.3	2.99E-20
SINE/B4|B4|4|41861171|41861469	-1.5	2.73E-20
LTR/ERVL-MaLR|MTD|4|41862178|41862303	-6.4	6.78E-21
SINE/B2|B2_Mm2|4|42006123|42006221	-1.5	1.95E-21
LINE/L1|L1MD2|4|42689041|42689329	-1.3	8.59E-22
LTR/ERV1|LTRIS2|4|41877124|41877612	-1.8	7.03E-22
LTR/ERVL-MaLR|MTEa|4|42689524|42689847	-1.1	4.80E-22
LTR/ERVL-MaLR|MTC|4|41859428|41859640	-7.2	2.79E-22
LINE/L1|L1MD2|4|42689848|42690320	-1.2	6.12E-23
LTR/ERVL-MaLR|ORR1A2|4|42695575|42695902	-1.4	3.42E-23
LTR/ERVL-MaLR|ORR1B2|4|41861679|41862023	-4.9	5.00E-24
LINE/L1|L1MdV_III|4|42682716|42684974	-1.2	4.51E-25
LTR/ERVL-MaLR|ORR1D2|4|41869118|41869231	-5.5	2.52E-27
LINE/L1|Lx5|4|41869274|41869392	-4.0	5.24E-28
LINE/L1|Lx9|4|41864119|41864457	-3.1	1.55E-28
LTR/ERVK|RMER17B2|4|42697077|42697999	-1.5	1.29E-28
SINE/Alu|B1_Mus1|4|41862664|41862806	-6.0	6.72E-32
LINE/L1|Lx5|4|41860065|41860499	-6.5	2.14E-32
LINE/L1|L1MD2|4|42690461|42691435	-1.2	6.41E-34
LTR/ERVK|RMER16-int|4|41880620|41881663	-2.0	1.18E-38
LTR/ERVL-MaLR|MTD|4|41863011|41863322	-6.8	1.33E-40
LTR/ERV1|MERV1_I-int~RLTR41|4|42685154|42688451	-1.2	8.05E-43
LTR/ERVK|RLTR40|4|21871708|21872365	-1.8	2.50E-45
LTR/ERVK|ERVB7_1-LTR_MM~ETnERV-int|4|41870907|41877123	-3.1	2.95E-48
LINE/L1|L1MEg|4|41866400|41866748	-5.6	2.14E-50
LTR/ERVL-MaLR|MTD|4|41864735|41864993	-4.3	1.66E-52
SINE/B2|B3|4|41865957|41866165	-5.1	8.07E-64
LTR/ERVL-MaLR|ORR1E|4|41868720|41868968	-4.6	1.22E-74
LTR/ERV1|RLTR1B-int|4|41877612|41880640	-2.1	4.96E-98

Table S2. qPCR probes and primers.

Taqman Probes	Assay Probe ID
Ifnb1	Mm00439552_s1
Ifng	Mm01168134_m1
Tnfa	Mm00443258_m1
Il1b	Mm00434228_m1
Il6	Mm00446191_m1
Ifit1	Mm00515153_m1
Ifit2	Mm00492606_m1
Ifi44	Mm00505670_m1
Isg15	Mm01705338_s1
Isg20	Mm00469585_m1
Zbp1	Mm01247052_m1
Oas1a	Mm00836412_m1
NP	Custom probe based on NC_002019.1 Assay ID:AIX02UC
Actin	Mm02619580_g1
Gapdh	Mm99999915_g1 (4352932E)
SYBR Green oligos	**Sequence**
M	F: 5'-CTTCTAACCGAGGTCGAAACGTA R: 5'-GGTGACAGGATTGGTCTTGTCTTTA from: Shin et al. 2013, Virology Journal 10:303
Gapdh	F: 5'-CATGGCCTTCCGTGTTCCTA R: 5'-CCTGCTTCACCACCTTCTTGAT from: Tsujita et al. 2006, PNAS 103:11946